August 2016

Dynamic Mechanical Analysis of Kissing Bonds in Bonded Joints

Tasha Graciano Graciano
University of Wisconsin-Milwaukee

DYNAMIC MECHANICAL ANALYSIS OF KISSING BONDS IN BONDED JOINTS

by

Tasha Graciano

A Thesis Submitted in

Partial Fulfillment of the

Requirements for the degree of

Master of Science

in Engineering

at

The University of Wisconsin-Milwaukee

August 2016

ABSTRACT

DYNAMICS MECHANICAL ANALSYSIS OF KISSING BONDS IN BONDED JOINTS

by

Tasha Graciano

The University of Wisconsin-Milwaukee, 2016
Under the Supervision of Dr. El-Hajjar and Dr. Anoop Dhingra

Inspection of kissing bond defects in composite structures is a challenge for traditional nondestructive testing (NDT) methods. A kissing bond (KB) is a bondline defect where two surfaces are in intimate contact with each other but with little to no bond strength. New nondestructive testing methods need to be developed that can detect adhesive kissing bonds, and areas within a composite joint where the bondline is compromised. The primary goal of this thesis is to explore if a NDT technique based on Dynamic Mechanical Analysis (DMA) can be established which is capable of detecting kissing bonds within bondlines in composite laminates that have been bonded with epoxy film and paste adhesives. DMA as a test method has the benefit that it can be conducted quickly and is able to test the material at various temperature and frequency ranges. Thirty specimens were prepared and attempts were made to create kissing bonds by introducing different types of contaminants at the bond location. Contamination used within the adhesive joint consisted of introduction of mold release and grease lubricant. Ultrasonic inspection is first performed to demonstrate that the surfaces were in contact in the bondline and no attenuation from porosity or delamination is present. Dynamic testing was performed on each sample in an attempt to detect these kissing bonds

using the DMA method. Information on changes in the sample's stiffness, storage modulus and loss modulus over a range of temperatures is recorded and analyzed. The specimens were subsequently tested in tension to determine the maximum strength of the materials. A geometrically nonlinear, 3D finite element (FE) analysis was performed to determine the stress and strain distributions within the composite single-lap joint (SLJ). The results obtained from the study showed artificial KBs appear to have been successfully fabricated based on tension testing and optical scans of fractured surfaces. Visual inspections of the fracture surfaces showed that contaminated bonds predominately failed via adhesion failure, while the control samples failed via cohesion. The production of KBs within the joints were more successful among the paste adhesive rather than the film adhesive. Analysis of DMA parameters shows a reasonable correlation for some of the parameters and the failure load. The FE results on the tension test showed that the stresses became increasingly higher within the single-lap joint for paste adhesive compared to the film adhesive. It was seen from the FEA models that the maximum shear stress and elastic strain occur near the overlap joint corners ends, suggesting that cohesive crack initiation is most likely to occur at the corners for defect-free samples. The stiffness results obtained from the DMA showed that all the paste samples had stiffness values much larger than the film samples; this elevated stiffness could contribute to the increased stress evident in the FE models. As the stresses were higher in the paste adhesive specimens, it is interpreted to be a contributing factor in the reductions of shear strength within the SLJs when defects are present.

TABLE OF CONTENTS

LIST OF FIGURES

LIST OF TABLES

LIST OF SYMBOLS AND ABBREVIATIONS

E: Young's modulus

E': Storage Modulus

E'': Loss Modulus

ν: Poisson's Ratio

τ: Shear Strength

KB: Kissing Bond

CFRP: Carbon-Fiber Reinforced Plastics

NDT: Non-destructive Testing

NDE: Non-destructive evaluation

DMA: Dynamic Mechanical Analysis

UT: Ultrasonic Testing

SLJ: Single Lap Joint

DCB: Double-Cantilever Beam

f_0: Force applied at peak

σ_0: Maximum Stress

ϵ_0: Maximum Strain

k: Specimen displacement

P_{max}: Maximum load at fracture

ACKNOWLEDGEMENTS

I would like to express my sincere and most gratitude to my professors, Dr. Anoop Dhingra and Dr. Rani El-hajjar, for their patience and intelligence. Throughout my whole graduate studies, I have learned both academic and practical knowledge from them. Both professors helped me in revising this thesis with great patience and encouragement. I want to thank Dr. Sadegh Shams for all his support and advices throughout my journey, he was always available whenever I had a questions and needed help. Lastly, I would also like to express my extreme gratitude to Dr. Tim Hunter, without whose help I would not have been able to finish my thesis. His insight and understanding of FEA modeling was a tremendous help to me and I cannot thank him enough.

1. Introduction

The demand for stronger, lighter structures in the aerospace and automotive industry has grown significantly over the last few decades. Due to their high strength to weight ratio, design flexibility and superior mechanical properties, advanced composite materials such as Carbon-Fiber Reinforced Plastics (CFRPs), have been widely implemented into these high-performance structural designs where high strength and stiffness are required at minimum weight [2]. Although there has been an increased usage of composites in the design of structural parts with high mechanical performance, there still remains a lack of understanding, especially with the use of composites in bonded joints [2].

Adhesive bonding is a widely used joining process in production of engineering products. Structural adhesive bonding as a joining technology provides many advantages in aerospace application [3]. A prerequisite for such an application is that the quality of the adhesive bond needed to be controlled [4]. There are several different types of defects that are known to occur in adhesive bonds that affect the load carrying capacity of an adhesive joint (see Fig 1.1). These defects can be split into three categories, voids inclusions, delaminations and low or zero volume kissing bonds (KB). A kissing bond is a special type of delamination

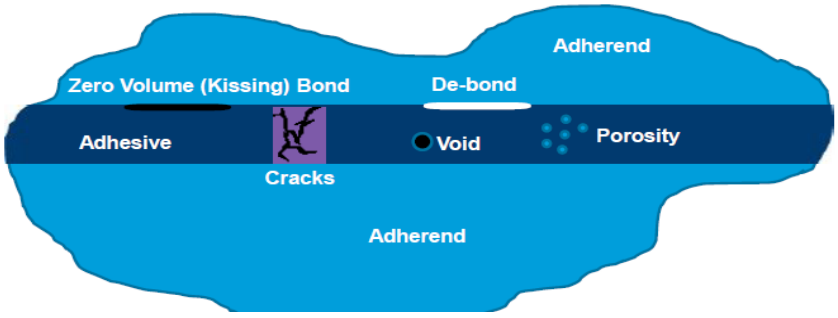

Figure 1.1: Defects that can occur in composite materials [1]

where there is no air pocket or void which can be detected using standard ultrasonic testing methods.

Voids, delamination and inclusions are easy to detect using a range of NDE (Non-destructive evaluation) techniques with the most common form of NDE being the C-scan ultrasound or X-ray radiography. However, no reliable NDT technique that is able to ensure the detection of a kissing bond, and by extension, ensure the quality of an adhesive bond. The level of understanding of the nature of kissing defects is not as robust as it could be, therefore sensitive and reliable non-destructive methods of detecting these defects in adhesive bonds must be developed in order to enable adhesive bonding to be used in primary structural roles [5]. One of the leading challenges to designing lightweight, cost-effective bonded structures is to detect kissing bonds when there are no other defects such as voids and cracks exist [6]. The lack of quantitative non-destructive testing procedures capable of detecting strength reducing defects such as kissing bonds is one of the limiting factors preventing the widespread use of adhesive bonding in the aeronautical industry[7].

1.1. Research Objective

The objective of any form of non-destructive test is to correlate qualitatively the joint strength with some physical, chemical or other parameter that can be measured without causing damage. This thesis investigates the effectiveness of a dynamic mechanical analysis (DMA) to successfully detect kissing bonds within bondlines in composite laminates that have been bonded with epoxy film and paste adhesives.

The research explores if the DMA method can be established as an effective tool in detecting the presence of KBs by studying the correlation between different DMA parameters

such as storage modulus, or stiffness. The information from these parameters is then used to correlate with the actual bond strengths measured when the samples were destructively tested. This thesis investigates the following:

i. The ability to successfully create kissing bonds within a carbon-fiber/epoxy reinforced single lap joint.

ii. Feasibility of using dynamic mechanical analysis to help identify presence of kissing bonds.

2. Literature Review

The following literature review covers the concepts of what exactly KBs are how they are classified in the scientific community and the fundamentals of dynamical mechanical analysis and how it can be used to evaluate such bonds. It also reviews previous research on the topic of ultrasonic testing of KBs.

The implementation of adhesive joints provides many benefits such as improved strength, corrosion resistance and improved durability. These benefits have permitted engineers to use bonded joints in areas that were dominated by mechanical fasteners. Thus, the ability to not only detect disbonds, but also to quantify the strength of bonded joints is critical to adhesive application in the automotive, aerospace and civil industries [8]. The exposure to pre-bond contaminations within the adherent-adhesive surface is believed to be one of the reasons why defects manifest themselves. Adhesives depend upon chemical bonds formed at the interface between the adhesive and adherent at the time the adhesive is cured. To understand adhesive bond failure, it is important to understand how adhesives function. If contaminations are present in the bondline and are not removed, they can result in a decrease of the surface energy, which will decrease the contact area between the adhesive and the bonding surface causing a decrease in shear strength [6]. As a result, the bond that is formed will not be able to carry load as both the substrates will in essence be only "kissing" one another with a near zero volume [6].

2.1. Kissing Bonds

A KB is a bondline defect where two surfaces are in intimate contact with each other but with little to no bond strength. These weakened bonds can deteriorate due to in-service loading or environmental conditions. The danger with KBs is that from the outside, they appear to be solidly bonded, but the bond strength between the two adherends is very low. A KB is an area of degrading interface that can cause a transition from a strong bond which fails by cohesion to a weak bond which fails by adhesion as illustrated in Fig 2.1 below [9].

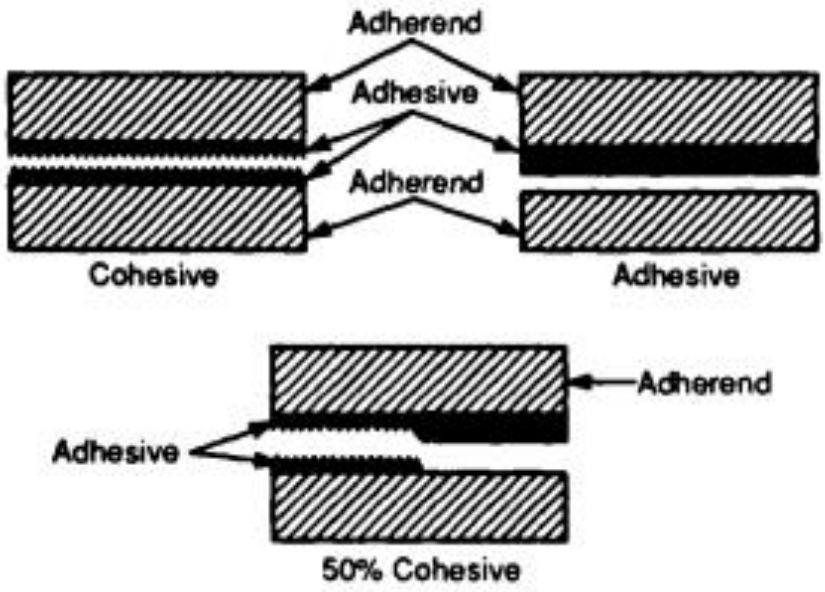

Figure 2.1: Cohesion, Adhesion and Mix-Mode Failure [9]

Adhesion failure is fracture at the interface between adhesive and adherend, while cohesion failure is fracture in the adhesive so that a layer of adhesive remains on both the adherends. A third form of failure that can be seen to occur in the specimens is a mixed-mode fracture. A Mixed-mode failure exhibits some cohesion and some adhesion failure because the interface is partially degraded [9]. The failure in this case exhibits areas of smooth surface as

well as areas which are rough and the strengths of adhesive bonds exhibiting mixed-mode failure is lower than the cohesion failures strength [9]. Ideal bonding should result into a ‘‘cohesive failure’’ as the maximum strength of the materials comprising the joint has been reached [10]. It is believed that most KBs result from poor surface preparation of as-molded surfaces due to excess fluorocarbons, silicones, plasticizers and such chemicals substances introduced from the manufacturing process [6]. Physically, KBs are low volume defects that have material properties that are similar to the surrounding material therefore they do not provide sufficient contrast to be detected using typical NDE procedures [5].

In order to simulate kissing bonds for further investigation, a protocol that reliably controls all these factors that could affect the normal bonding process needs to be fabricated. Regardless of their origin, defective bonds must exhibit certain characteristics to be regarded as possible reference samples for kissing bonds. These criteria, although partly arbitrary, are derived from what we understand from the real nature of kissing bonds and are as follows [11]:

1. The strength in a lap shear test must give a reduction in shear strength of the bond by 80% for the defect if over the entire bond, or have a reduction in strength by 50% for small patches in the bonded area.

2. The mode of failure must be adhesive, which is purely at the interface between the adherent and adhesive.

3. They must be undetectable from normal bonds with ultrasonic C-scans.

Simulated KBs can be produced in two ways, dry contact and liquid contact. Dry contact bonds are achieved by compressively loading an adherend to a pre-cured adhesive to achieve intimate contact with zero adhesion across the entire bond [5]. A liquid layer bond is a kissing defect created by adding a small amount of contaminant to the bond line. In this research, we are specifically investigating the effect of a liquid layer bond defect.

2.2. Mechanical Behavior

The evaluation of new materials and predicting their performance for specific applications is a challenging one for both engineers and designers. The dimensional and mechanical stability of materials is of paramount importance to their use in the everyday world where they may encounter a wide variation in temperature through design or by accident [12]. In the world of composites, there are several different techniques used to study the relationship between a material's dimensional and mechanical properties and its temperature.

DMA is a thermal analysis technique that measures the properties of a material as they are deformed by the application of oscillatory force at a set frequency in a cyclic manner [13]. Most DMA measurements are made using a single frequency and constant deformation amplitude while varying temperature, however, variations in amplitude and frequencies can provide further information [13]. This allows the material's response to stress, temperature, frequency and other parameters to be studied [14]. DMA involves applying a variable sinusoidal stress to a sample of known geometry and the resultant sinusoidal strain is measured [14]. The sample can be subjected to a controlled stress or strain in order to obtain modulus information. The response of a material to the stimuli is divided into an elastic

response or storage modulus (E'), and a viscous response (E"). The elastic response or storage modulus is an in-phase component that accounts for the elastic energy stored in the material due to the dynamic response, and the loss modulus is representative of the viscous response or out of phase component that measures the energy dissipated in the material due to friction and internal motions [15]. The ratio between the loss and storage modulus gives a useful quantity known as the mechanical damping factor, tan (δ) which is a measure of the amount of deformational energy that is dissipated as heat during each cycle and it tells us how good a material will be at absorbing energy [14].

Damping is a property that characterizes energy dissipation in dynamically loaded structures and materials, and the internal damping of a material is quite sensitive to the micro-structure detail of the material [16]. Given that damping is so sensitive to structural integrity, damping methods have been used as part of the means to analyze damage in composite materials as early as when the shift of engineering materials from metallic to nonmetallic composite materials began in the 1970s [16]. The position and height of the tan (δ) peak is indicative of the structure and properties of a composite material. According to [17], a stronger interface (i.e. , defect free) allows less dissipation. Therefore, if we observe high tan (δ) for a sample, it can be interpreted as an indication that a weak bond or KB may be present within the bond. Damping tends to reduce at the interface whenever there is a higher degree of interaction or adhesion between the constituents [17].

The expressions for storage modulus, loss modulus and damping are given as [15]:

$$E' = \frac{\sigma_0}{\epsilon_0}\cos\delta = \frac{f_0}{bk}\cos\delta \qquad [2.1]$$

$$E'' = \frac{\sigma_0}{\epsilon_0}\sin\delta = \frac{f_0}{bk}\sin\delta \quad [2.2]$$

$$\tan\delta = \frac{E''}{E'} \quad [2.3]$$

Where f_0 is the force applied at the peak of the sinusoidal wave, k is the specimen displacement at the peak, b is the specimen geometry term, σ_0 and ϵ_0 are the maximum stress and the strain at maximum stress respectively and δ is the phase angle between a sinusoidal applied stress and a measured strain. Different parameters such as frequency, stiffness, tan delta and variations in the amplitude of the response signals from the adhesive joint are criterion for the understanding of the quality of the adhesive joint and could be used to help detect defects present in the material.

2.3. Ultrasonic Testing

Ultrasonic testing (UT) is an established non-destructive testing technique for detecting subsurface damage in composites [3]. When ultrasonic waves travel through composite materials, the wave propagation is influenced by internal damage, which acts as discontinuities and introduce a local change in acoustic impedance [3]. In UT, high frequency sound waves are generated by a transducer and transmitted into a test object to obtain information about the object without altering or damaging it in any way [18]. High frequency waves are more sensitive to defects: low frequency waves can penetrate to greater depths [3]. The test may be carried out with either a single transducer in pulse-echo mode or two transducers in through-transmission mode [19]. Pulse-echo method is applicable where inspection access is limited to one side of a structure. In this inspection method, a single

transducer operating as a transmitting-receiver is scanned in a plane parallel to the specimen surface detecting acoustic signal from the front and back surfaces of the specimen, and from discontinuities or defects present in the specimen [18]. Through-transmission uses two separate ultrasonic transducers (i.e. transmitter and receiver) facing directly opposite each other and separated by the specimen. Defects in the specimen will either block or attenuate the transmitted signal thus indicating the presence of a defect or internal flaw. UT as an NDE technique is known for not being able to detect changes in the adhesive bond strength, nevertheless it yields information regarding the morphological and elastic features at the interface of adhesive bonds by their behavior in the material inspected [4]. For this investigation, through transmission UT was used to analyze the integrity of the samples.

Two basic quantities are measured in ultrasonic testing:

1. Time of flight or the amount of time for the sound to travel through the sample.

2. The amplitude of the received signal.

When a KB occurs in localized spots surrounded by more-or-less well-bonded areas, sufficient compressive residual stress might persist at the defective interface to hide it from low-level ultrasonic NDE until it is turned into an actual delamination by excess loads [20]. KBs produce very low contrast in ultrasonic inspection since there is an intimate mechanical contact between the counterparts without an actual bond[20]. A high-frequency, high angle inspection is suggested to increase the detectability of KBs at adherend-adhesive interfaces [20].

2.4. Summary

A comprehensive literature review was conducted in order to understand the nature of kissing bonds and their mechanical behavior. An overview on the fundamentals behind UT and DMA techniques was presented in order to understand how these NDT techniques work and what information we can expect to obtain from them. The parameters that are obtained from DMA testing are presented and explained as well as the specific UT method chosen for this study. With this information explained, we can move on to the experimental portion of the study where we try to recreate these defects within composite samples by introducing contaminants to the bond area.

3. Experimental Method

The following section covers the process used to manufacture the test coupons for this experiment, along with detailed layup and material information for the adherend, adhesives and contaminations. The chapter also discusses the ultrasonic inspection of the fabricated specimens.

3.1. Experimental Procedure

The physiochemical parameters that may influence strength loss within a bonded joint may be divided into two groups, manufacturing-related parameters and in-service-related parameters [21]. In this study, we focused on manufacturing-related parameters and considered two pre-bond contaminations namely a mold release agent and a grease lubricant that can commonly appear during manufacturing of an adhesively bonded joint.

To begin, the contaminants were applied to one of the adherend while the adhesive was applied to the other. For the mold release contaminant, EpoXease mold release was used (Slide Products, Wheeling IL). Release agent is a chemical used to facilitate easy removal of molded or cast parts from the molds [22]. These agents are applied to the contact surface of the mold prior to casting or molding, however, it was noticed very early more than 30 years ago, that residues of release agents on such CFRP surfaces are responsible for bond line failures and poor mechanical performance [10]. For the grease contaminant, small amounts of Polylube 1000 (ParkTool, St. Paul, MN) which is a high performance polyuria grease was used.

3.2. Specimen Preparation

The test specimens used in the research were fabricated from a 3-ply panel of carbon fiber/epoxy prepreg plain weave composite pre-impregnated with epoxy resin(prepreg) sheets using T700SC-12K-50C/#2510 (Toray Industries; Chuo, Japan). This prepreg material has a nominal ply thickness of 0.21mm. For bonding purposes, two different adhesives were used, first an epoxy-based structural adhesive film AF163-2 (3M; St. Paul, MN), with a curing process done in a Wabash GE301t-15-Bcx compression molding hot press, and a paste adhesive, Huntsman Epibond 100 A/B, with the curing done in a model 30GC lab oven. The material properties for the composite material and the adhesives, as provided by the manufacturers are presented in Tables 3.1 and Tables 3.2, 3.3.

Table 3.1: Mechanical Properties of T700GC-12K-50C/#2510 Prepreg

E_1 GPa (Msi)	E_2 GPa (Msi)	v_{12}	G_{12} GPa (Msi)	Ply thickness mm (in)
57.2 (8.3)	55.8 (8.1)	0.037	4.00 (0.58)	0.21 (0.0085)

Table 3.2: Room temperature Film adhesive material properties [23]

E (GPa)	v	G (MPa)	Tension Strength (MPa)
1.11	0.34	0.413	48.2

Table 3.3: Room temperature paste adhesive material properties [24]

E (GPa)	v	G (MPa)	Tension Strength (MPa)
2.17	0.22	897	51.7

The first challenge in this study was to be able to artificially create the weak bonds or KBs within the adhesive-adherent joints in such a way that the strength results would be repeatable with some small level of variation. This was done by fabricating a series of single lap joint (SLJ) coupons that are made with CFRP adherend with a 25-mm x 9.5 mm kissing bond areas as shown in Figures 3.1 and 3.2.

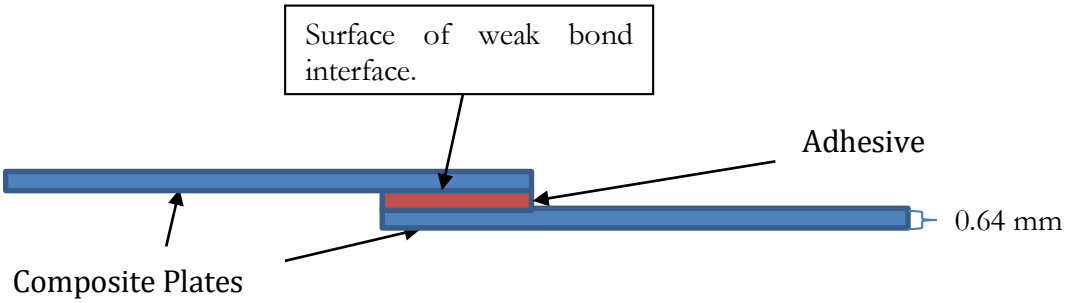

Figure 3.1: Schematic of Single Lap Joint Specimen

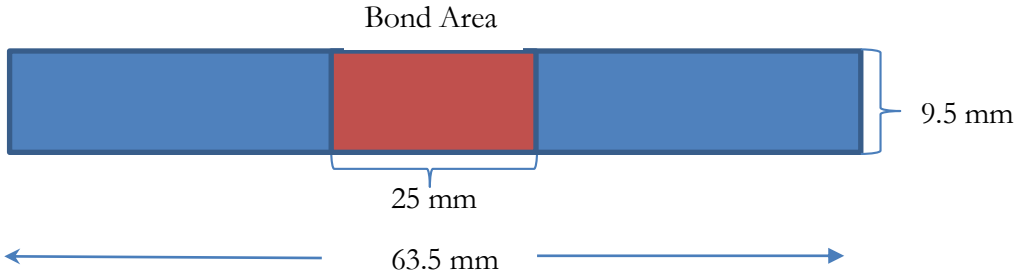

Figure 3.2: Weak Bond Area

All CFRP coupons are nominally of 63.5 mm length, 9.5 mm width, with a 0.64 mm thickness. The bonded specimen thickness was roughly 1.31mm for film adhesive specimens and between 1.43 mm & 1.51 mm for paste adhesive. According to [24], a layer of paste adhesive 0.1 to 0.3 mm thick will normally provide the maximum lap shear strength, however, this adhesive has been designed to be effective in layers up to 3 mm so the specimens were

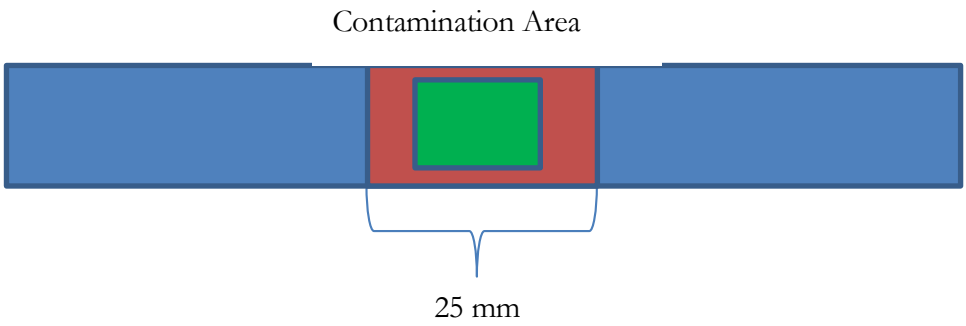

Figure 3.3: Contamination Area

within these tolerances. Using an identical layup procedure, samples were created with the varying contaminants. It is known that one of the basic requirements for a good bond is the roughness and cleanliness of the adherend surface created by sanding, the roughened surface creates better mechanical interlocking between adhesive and adherend [16]. Therefore, before introducing the contaminations onto the bonding areas, the area is treated in the following procedure. Each sample was slightly roughened with 100 grit sandpaper and then wiped clean with isopropyl alcohol. Contaminants were applied to one side of the adherend in the lap overlap region and allowed to dry for a period of 5 minutes at room temperature before bonded into a lap joint structure in order to produce changes in the interface properties between the CFRP and adhesive. The mold release agent was applied to the surface of the adherend by means of a spray can and then spread within the bonding area concentrating within the center of the bond area trying to keep minimal residual contaminate around the edges. The grease was applied in a single layer and localized within the center area as well.

Six groups were created with five specimens in each for a total of 30 samples. For the first set of 15 samples, one layer of AF163-2 film adhesive was used for bonding, while the two-part Epibond 100 A/B paste was used for the second set of samples as illustrated in table 3.4 below. Tabs were used to ensure the accuracy of the tensile strength specimens and were applied to the tension strength specimens in accordance with Section 3.1.4 of the AGATE "Material Qualification Methodology for Epoxy-Based Prepreg Composite Material System", dated February 1999. Following the curing process, a visual examination of the sample was carried out and then scanned using UT to check for porosity or other defects.

Table 3.4: Description of sample groups and tested specimens

Group	Adhesive	Contamination	No. of Specimens	Cure Method
1	Film	Control	5	Hot Press
2	Film	Mold release	5	Hot Press
3	Film	Grease	5	Hot Press
4	Paste	Control	5	Oven Cured
5	Paste	Grease	5	Oven Cured
6	Paste	Mold release	5	Oven Cured
		Total Specimens	30	

3.3. Experimental Procedure Summary

Thirty single-lap joint samples were fabricated using carbon fiber/epoxy prepreg plain weave composite sheets. For bonding purposes two different adhesives were used, one an epoxy-based structural adhesive film, and the other a two-part epoxy paste. To artificially simulate kissing bonds, two different contaminants were introduced into the bond area, a

grease contaminant and a mold release agent. After curing, the samples were tested via DMA and tension testing. These results are given in the next chapter.

4. Results and Discussion

In the following section, attempts were made to simulate defective bond conditions to support development of bond-strength measurements by nondestructive methods such as UT or DMA. The objective of any form of non-destructive test is to correlate qualitatively the joint strength with some physical, chemical or other parameter that can be measured without causing damage. The storage modulus, stiffness and ultrasonic attenuations from test samples are then correlated to the actual bond strengths measured when the samples were destructively tested. Properly correlating specific NDE parameters to the results obtained through the destructive test, a bond quality gauge could be developed for each type of bond and geometry.

4.1. C-Scan Ultrasonic Testing

UT inspection was used to study the presence of KB in the bonded joints. The reader is referred to section 2.3 for a description of this method. If KBs were created by the addition of contamination at the interface between the adherent and the adhesive, it must be verified that it is the only source of bonded joint reduction and that porosity or delaminations are not present in the joint. Bonded joint samples were subjected to normal incidence water immersion ultrasonic scanning in through-transmission mode using a 10 MHz focused transducer in the attempts to acquire the highest feasible inspections possible. The ultrasonic set up used was a TecScan computer controlled ultrasonic pulser/receiver (TecScan, Montreal, Canada) illustrated in Figure 4.1 below.

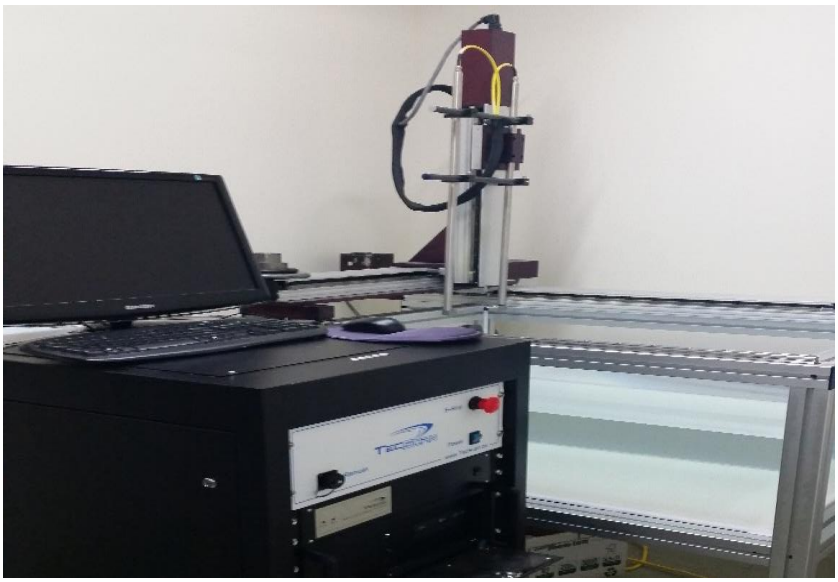

Figure 4.1: TecScan Computer Controlled Ultrasonic Immersion tank

The bonded joint area was observed using a thru-transmission UT method using a pair of 10MHz transducers. In order to establish a baseline for the UT sample for comparison purposes, a few samples were prepared with intentional delamination or UT visible voids. Sandwich style set-up using pressure sensitive tape (Airtech, Huntington Beach, Ca) and Teflon film were created and placed within the bond area as illustrated in Figure 4.2 below. The defect simulates an air bubble within the joint that should be clearly noticeable in the C-scan. The inspected data is color-coded and can be noted that the general brightness of the C-scan darkens as the bond becomes weaker (higher attenuation, lower amplitude). The images do not allow for exact bond strength based on the color codes; however, they do significantly

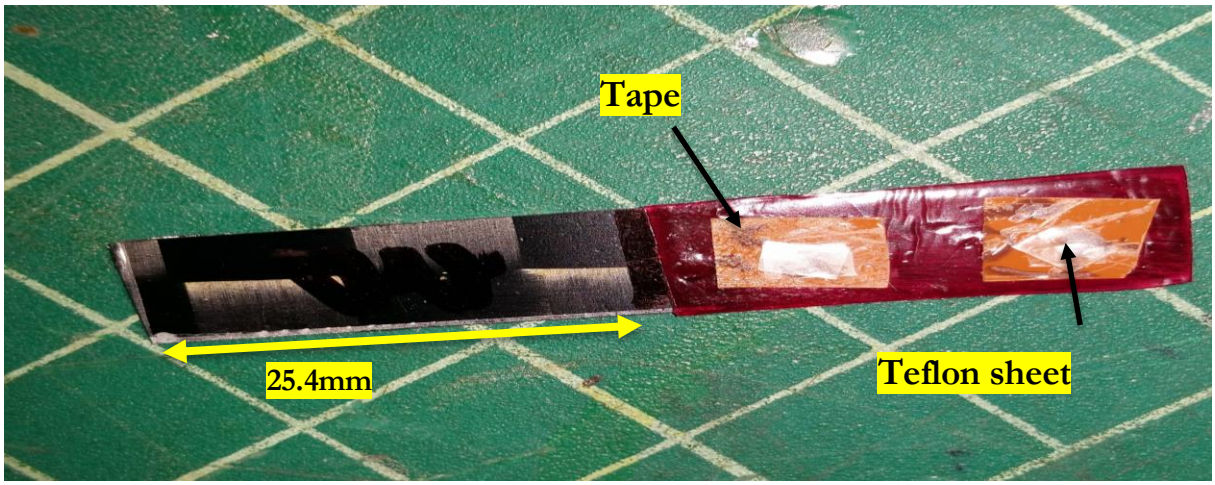

Figure 4.2: UT Specimen with Tape/Teflon Sandwich Contamination

change when the bond strength drops. We can see in Figure 4.3 below that the areas where the tape/teflon defect was located exhibited an area of high attenuation. This area is a clear indication of a delamination or weak bonding location in coupon (a), it appears that the bottom void may not have been properly sealed allowing the air trapped inside to escape and thus not

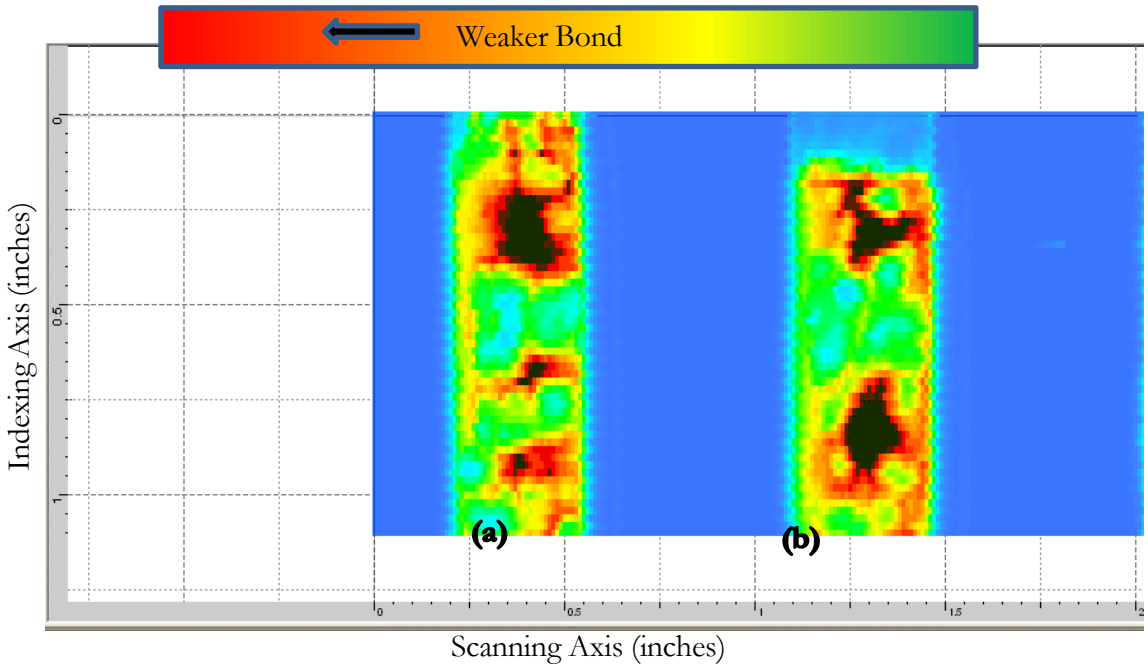

Figure 4.3: UT SLJ with Tape-Teflon Sandwich
(Red regions have higher attenuations)

creating a significant void compared to the defect above it. Some of the signal was able to pass through the sandwich set-up in certain areas while in others noted by the black region it clearly was dampened. Areas where the signal traveled through the tape itself and not the Teflon piece appear to have dampened the signal as well appearing orange and red in the scan signifying that the area may have bonded but the strength of that bond was drastically weaker than the surrounding green regions.

Next, we looked at the film SLJ, looking at the three specimens from left to right, (defect-free, mold release, and grease) we can see that there was a more consistent attenuation in the C-scans for both the mold release specimen and the grease. The resulting C-scan images from the film and paste samples are shown in Figure 4.4 and 4.5. There is some indication of attenuation present within the specimen; however, this information is insufficient to prove the presence

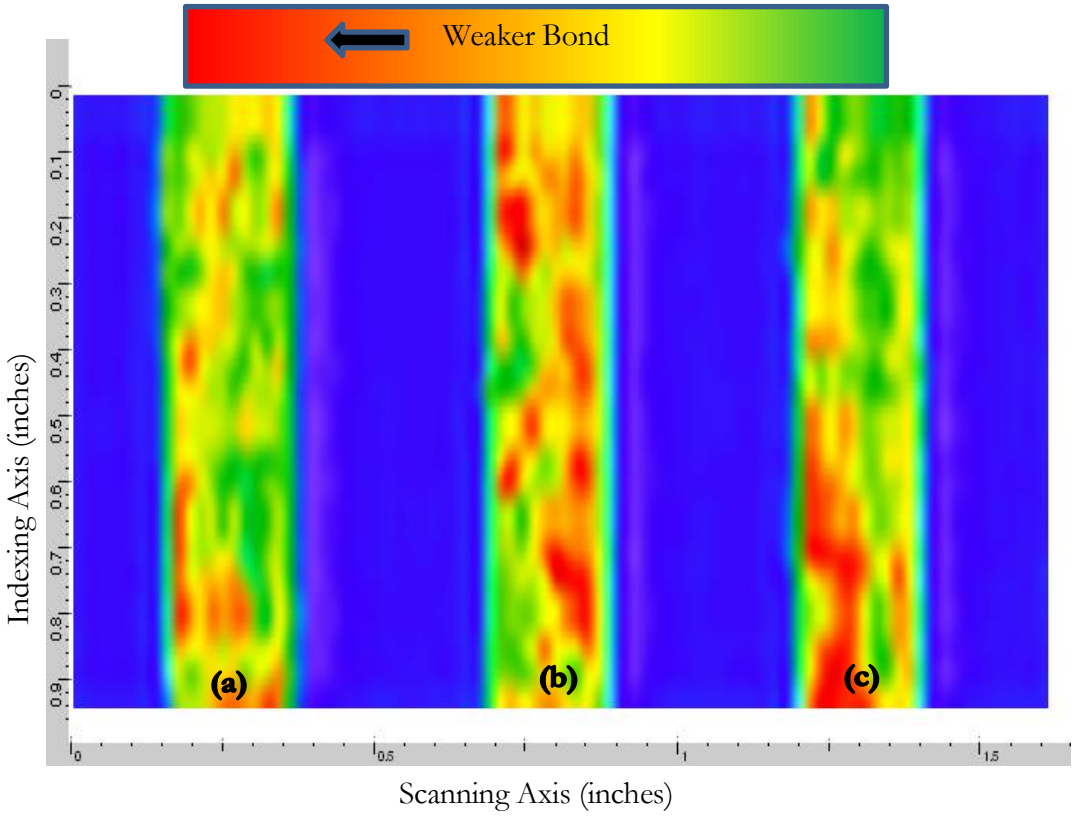

Figure 4.4: UT of Film adhesive SLJ, (a) Control, (b) Mold Release, (c) Grease

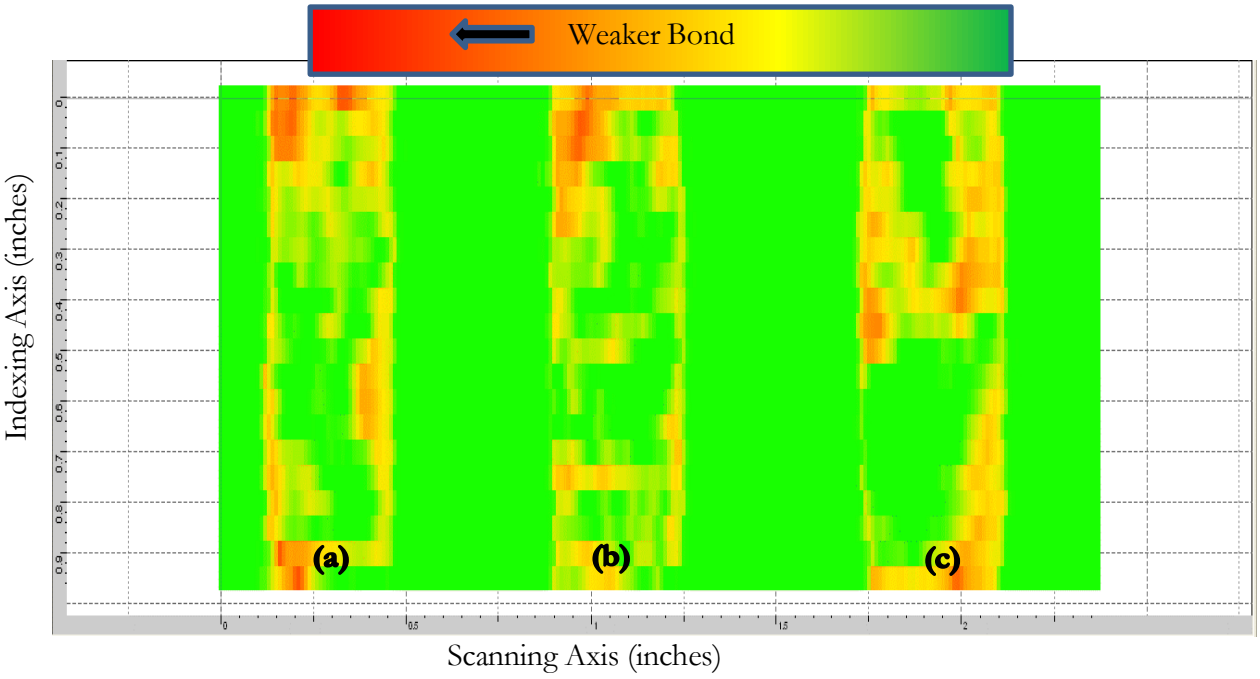

Figure 4.5: UT of Paste SLJ, (a) Control, (b) Mold Release, (c) Grease

of KBs. Similar trend can be observed in the presence of cohesion defects like voids and porosity. Scans of the paste adhesive bonded joints were also subjected to normal incidence water immersion ultrasonic scanning in through-transmission mode using a 10 MHz focused transducer in an attempt to acquire the highest feasible inspections possible. We can see from the scan in Fig 4.5, above, that there was very minimal attenuation within the bond area when tested, the bright green area is an indication of a good bond quality and no present defect meaning the signal was able to travel straight through the specimen and received by the transducer on the other side with no interference. The yellow and red regions can be interpreted as areas of slight degradation or reduced amplitude in the signal process but cannot be considered a representation of kissing bonds within the sample. Based on the UT testing results, it is concluded that satisfactory bonding quality was achieved confirming the statements that conventional NDT cannot detect kissing bonds or heavily contaminated bonds. The same specimens are next examined using the DMA method.

4.2. DMA Testing

In this section we assess whether the DMA can be used to detect if the contamination in the bonded joint changes the elastic and viscous response. Mechanical testing using a double-cantilever beam (DCB) setup was carried out on a Q800 DMA system (TA instruments, New Castle, Delaware) as shown in Fig 4.6 below.

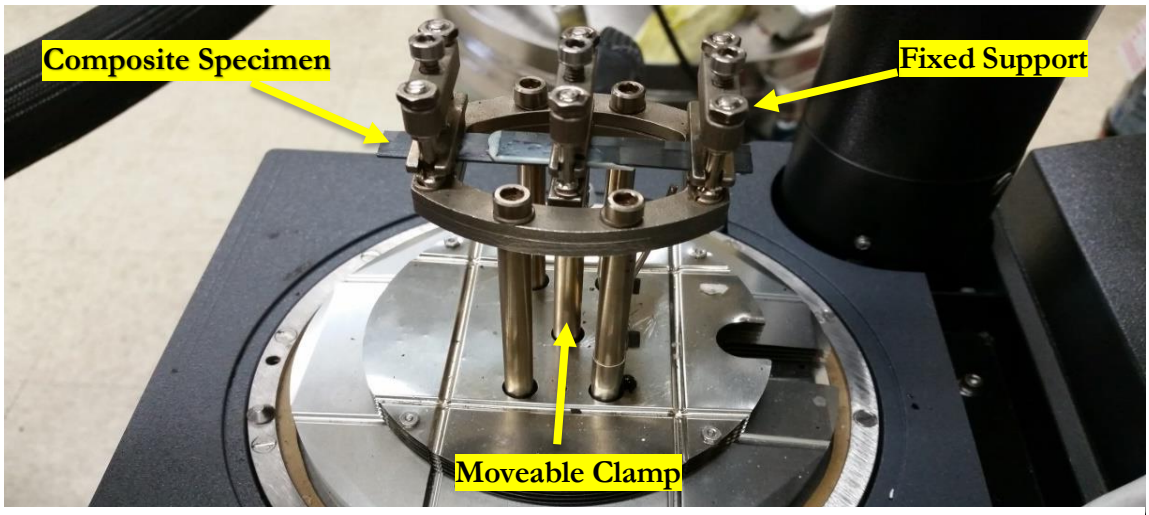

Figure 4.6: Double Cantilever DMA Test Setup

The test specimens were approximately (63.5 mm x 9.5 mm x 1.40 mm) in length, width and thickness respectively. The specimens were subjected to two types of tests. The tests consisted of a controlled displacement (15 μm) and temperature ramp profile of -70 to 220 °C at a rate of 5°C/min with a constant frequency of 1.0 Hz. In this study, a controlled displacement was used to distort the specimen surface in order to obtain the stiffness, storage modulus (E'), loss modulus (E"), and tan (δ) values of the composite specimen for analysis.

4.3. Tension testing

The difficulty with KBs is that no matter how good the procedure for producing them is, one is never 100% sure that the sample used contains a KB; therefore, a destructive lap shear static test is needed [11]. When proceeding to such a destructive test, a series of good bonds need to get broken in order to establish a baseline for the strength value [11]. Only samples that exhibit a reduction in joint shear strength of at least 50% and that had pure adhesive mode of failure will be classified as a KB. Hydraulic fixtures with end tabs bonded on either side were used to grip the adhesive joint samples. Both the film and paste adhesive joint samples were loaded until failure in a testing machine of 88 kN capacity subjected to loading rate of 0.05 in/min.

The joint adhesive strength is calculated using the following formula:

$$\tau = \frac{P_{max}}{A} \qquad [4.1]$$

where τ is the adhesive strength, P_{max} is the maximum load at fracture, and A is the average cross-sectional area. The average failure loads and shear strength of the control joints and those containing defects for the film SLJ are presented in Table 4.1 below.

Table 4.1: Average failure load of tested film samples

Contamination	Failure Load (kN)	Shear Strength (MPa)	Adhesive Area (mm^2)
Control (no defect)	3.44 ± 0.74	14.484	237.5
Mold release	3.09 ± 0.32	13.010	237.5
Grease	1.83 ± 1.17	7.705	237.5

From the information noted in table 4.1 above, we can see that the addition of the grease contaminant to the bond area on average significantly reduced the failure load and shear strength of the joints by approximately 46% while the mold release only reduced the shear strength of the bond by approximately 10%. This occurrence could be attributed to the fact that the mold release contaminant used was a silicone free substance unlike the silicon mold release that is known to cause a much larger reduction in adhesion. According to [5], it is considered that a reduction in joint strength of 50% for this type of defective joint indicated kissing defect.

Our hypothesis was that the samples with contamination should have lower shear strength when compared to the shear strength of the control sample. However, based on the data collected from the samples during tension testing, the mold release contaminant does not appear to influence the bonding strength as much as the grease. A theory as to why this happened within the contaminated samples could be traced back to the curing process. If the contaminant is squeezed out of the joint during curing, the result is that the KB closes up under the load; therefore, essentially making its bonding similar to that of a control sample without any contamination defects. As it is apparent from the similar shear strengths of the samples listed in table 4.1 above, it is believed that this is a possible reason for what occurred thus failing in creating any kissing bonds. Another reason for the mold release samples to fail at a larger than expected load could be that there was a strong chemical reaction between the lubricant, adherend and adhesive providing structural strength. For cases when a mold release sample failed at larger loads, a mixed-mode failure was observed on the surface of the composite.

Next, we looked at how the contaminations affect the mechanical properties of single lap joints bonded with the two-part paste adhesive. From the information noted in table 4.2 below, we can see that the addition of the grease contaminant to the bond area in the paste joints reduced the failure load and shear strength of the joints by approximately 62% which was slightly greater than that which occurred using the film adhesive. The presence of the mold release had a larger effect on the paste bonding integrity of the joint compared to the film with a reduction rate of approximately 51%.

Table 4.2: Average failure load for paste adhesive lap Joints

Contamination	Failure Load (kN)	Shear Strength (MPa)	Adhesive Area (mm^2)
Control (no defect)	1.95 ± 0.37	8.210	237.5
Mold release	0.95 ± 0.35	4.000	237.5
Grease	0.74 ± 0.26	3.115	237.5

Within both categories of adhesives (i.e. paste and film) there appears to have been successful production of KBs. For the film adhesive samples, successful KBs appear to have been created in the grease samples while failing to create KB in any of the mold release samples. For the paste samples, there was successful production of KBs in both contaminants. Therefore, the question we are left with is why KBs could be produced within mold release paste adhesive samples but not film adhesive. We believe that although the mold release being used in this study does not contain silicon, which is prone to affect bonding in adhesive joints,

its chemical composition somehow alters or interacts with the material makeup of the paste adhesive causing it to lose bonding strength with the adherend.

The identification of the type of failure of the bonded joint provides significant information to understand the failure mechanisms that took place. As mentioned in section 2.1, the three basic mechanisms of failure in adhesively bonded joints are ‘‘cohesive failure’’, ‘‘adhesive failure’’ and ‘‘Mixed-mode failure’’. In most cases, a combination of thin-layer

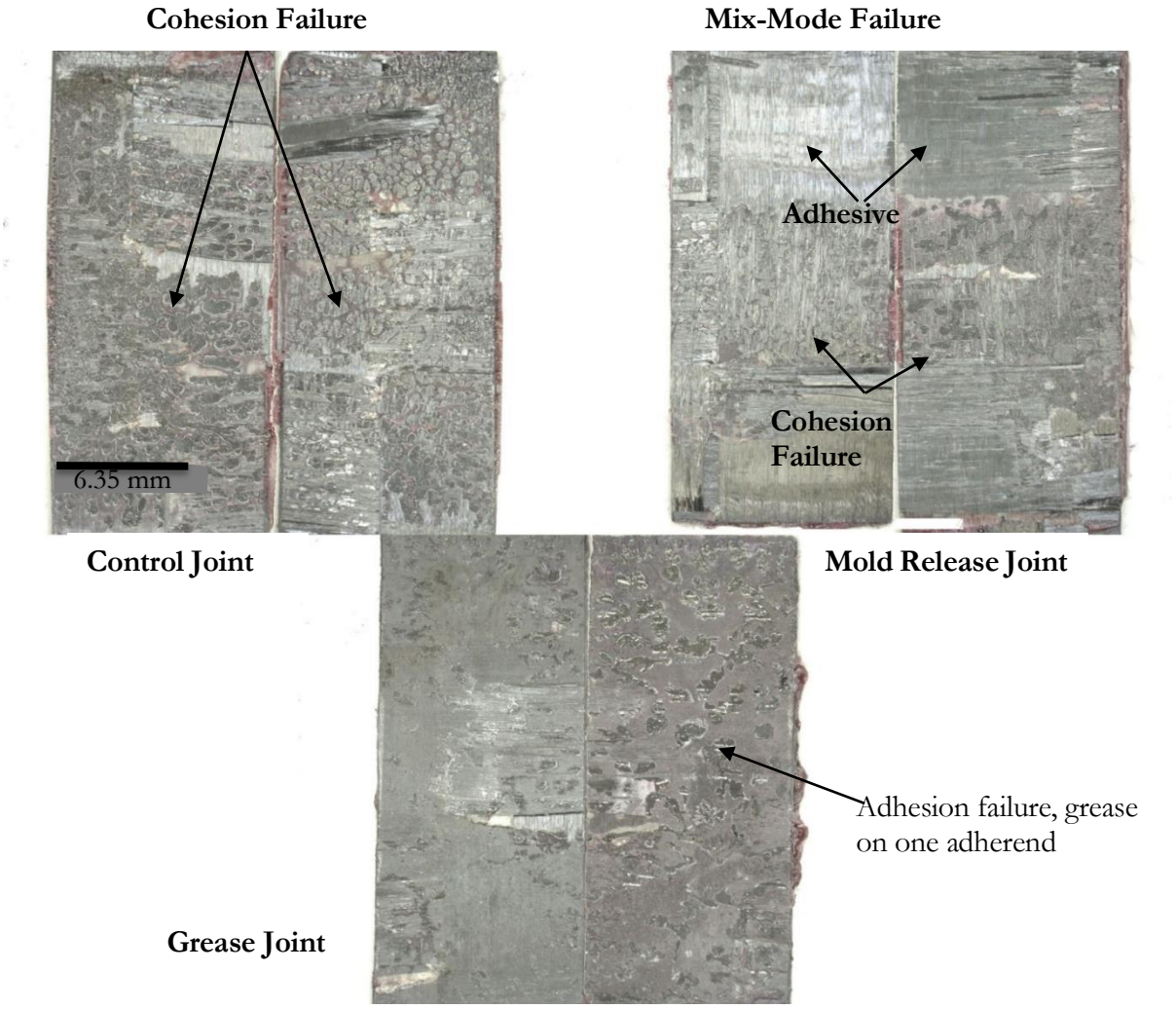

Figure 4.7: Shows both sides of adhesive joint in the bondline region.

cohesive failure and light-fiber-tear failure modes was observed.

In this study, an identification of the failure or fracture mode for each scenario was done in order to assess the effects of the contamination on the quality of the adherend/adhesive interface. From the scans in figure 4.7, it can be seen that the defect-free bonded film adhesive joint or control joint, failed via cohesion failure, which demonstrates good adhesion between the adhesive and adherend. The contaminated bonds predominately failed via adhesion failure that is exactly what we wanted to see, however, there were some mold release samples that failed via mix-mode method. Visual inspection of the grease adherends showed that the bulk of the adhesive remained attached to one adherend. In the case of the grease joint, the grease prevented adhesion between adherends and adhesive in the area where it was applied on one adherend only, the adhesive remained bonded to the other adherend. This initially suggested that adhesive failure or failure along the composite-adhesive interface was the principal damage mode. A combination of thin-layer cohesive failure and light-fiber-tear failure modes was observed.

As mentioned earlier, to be classified as a kissing bond; failure mode must be by adhesion failure. A good bond would fail cohesively within the adhesive layer, which is what we expected to occur during testing in the control sample. However, because some bonds that fail adhesively can exhibit greater mechanical strength than a similar joint bonded with a weaker adhesive, which fails cohesively, determining quality based on the failure mode is not recommended [25] The mold release appears to have affected the adhesive and prevented adhesion of the adhesive to the adherend. Signs of mix mode failure appear to manifest in the mold release samples, signifying that failure occurred due to both adhesive and cohesive failure. Due to the apparent failure type, mold release was not suitable for introducing a controlled simulated kissing defect.

Looking at the fracture surface of the paste adhesive single lap joints illustrated in the scans in figure 4.8, it is apparent that failure modes for this adhesive were different for the contaminants. Visual inspection of the grease adherend showed that the bulk of the adhesive

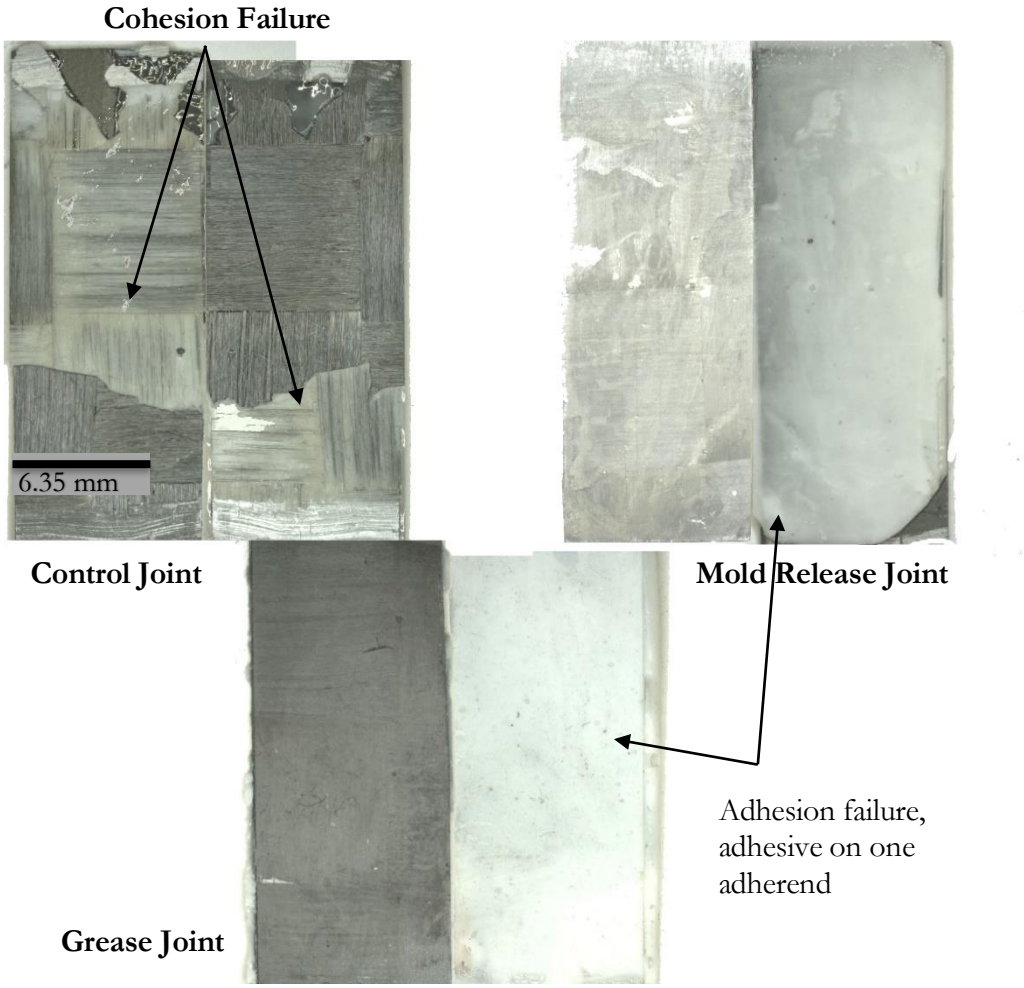

Figure 4.8: Fracture surfaces of Paste adhesive SLJ specimens

remained attached to one adherend that is a good indication of adhesion failure. However, unlike the results of the film adhesive SLJ, the mold release samples all appeared to fail by pure adhesive failure as well instead of mix-mode.

4.4. Summary

In summary, attempts to simulate defective bond conditions to support development of bond-strength measurements by DMA are performed. Artificial KBs appear to have been successfully fabricated based on tension testing and optical scans of fractured surfaces. Visual inspections of the fracture surfaces showed that contaminated bonds predominately failed via adhesion failure that is exactly what we wanted to see, while the control samples failed via cohesion. The production of KBs within the joints were more successful among the paste adhesive rather than the film adhesive SLJs. A statistical analysis of the parameters obtained from DMA testing, storages modulus, stiffness and tan (δ) to determine some correlation with failure loads from the single lap joint tension testing is presented next.

4.5. Statistical Method

Determining the relationship between two random variables, if one exists, is very important as it gives the experimenter the ability to make predictions about one variable relative to the other. In this section, a regression analysis represented by the scatter plots below, was conducted in order to establish the relationship between the parameters obtained from DMA for all samples and the failure strength of the samples obtained during tension testing. A correlation analysis was also performed to measure the strength of the relationship between the parameters. The objective of doing such an analysis is to see if in fact a correlation between the data collected from two test methods could give insight into the strength of the bond. The correlation coefficient is always between -1 and +1. The closer the correlation is to ± 1, the closer the linear relationship is between the variables being considered [26]. The correlation coefficients are interpreted as such:

Table 4.3: Statistical parameters used in analysis of data

Coefficient range	Direction of Relationship
-1.0 to -0.7	Strong negative association-variable tend to move in opposite directions
-0.7 to -0.3	Weak negative association
-0.3 to +0.3	Little to no association
+0.3 to +0.7	Weak positive association
+0.7 to + 1.0	Strong Positive association- both variables move in the same direction, if one increases, the other does too.

The first parameter analyzed against the failure loads obtained from tension testing for the grease and mold release samples was the storage modulus obtained from the DMA testing. Four test specimens from each category (defect-free, grease, mold release) are illustrated in figure 4.9 below.

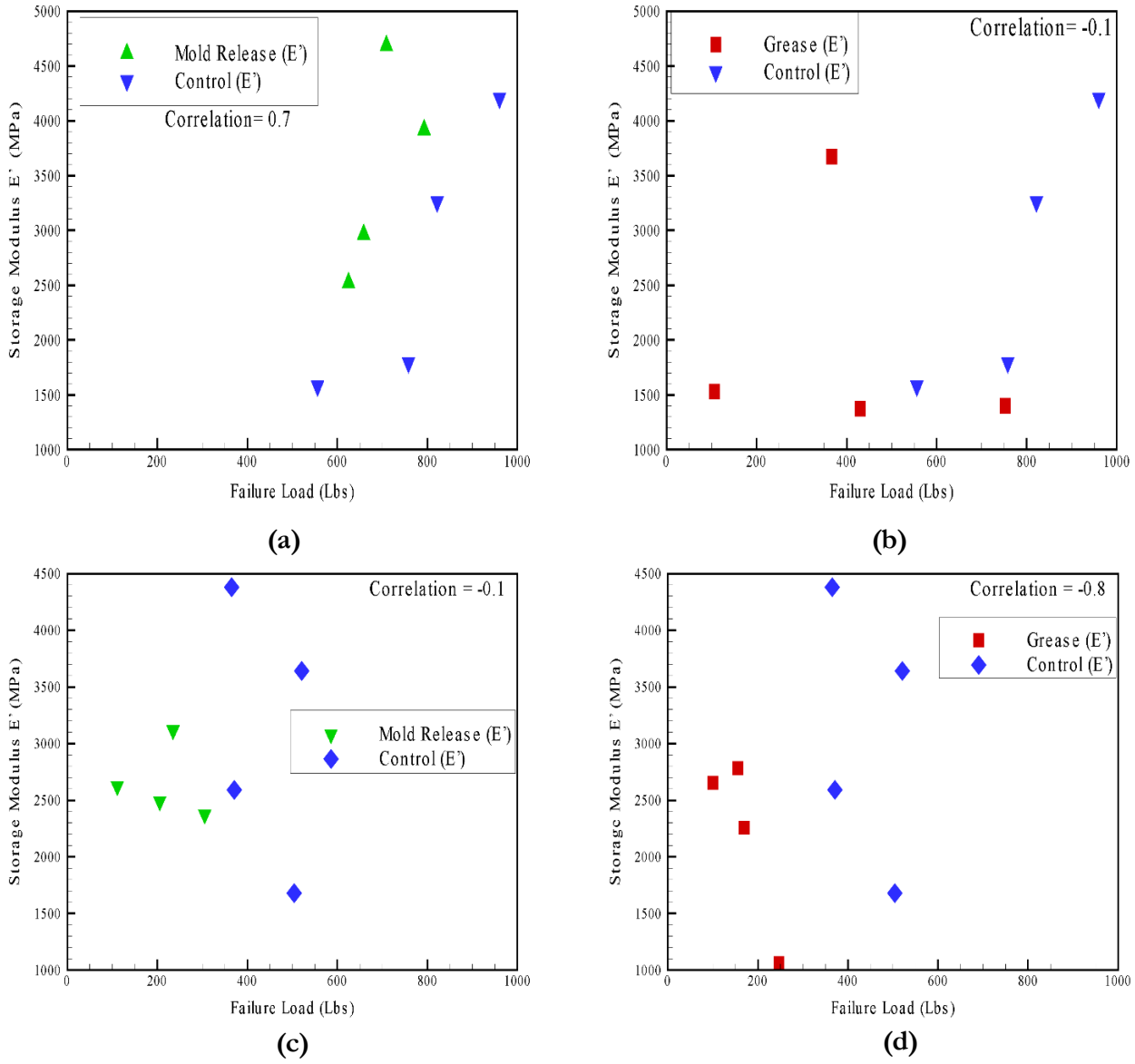

Figure 4.9: Storage Modulus E' vs Failure load for (a) Mold release film samples (b) Grease film samples(c) Paste mold release, (d) Paste grease contamination

For the analysis, we compared the storage modulus of each sample against the failure load and obtained the results illustrated in figure 4.9. Looking at fig 4.9 (a) and (b) for the mold and grease film adhesive samples respectively, we see that for the mold release contaminated specimens there was a weak positive relationship between the variables while for the grease there was no relationship at all. Samples with higher storage modulus values, possessed failure loads ranging on the larger scale. This observation can be interpreted as an indication that when the storage modulus value is high the sample possesses a stronger adhesive bond and it therefore, does not contain any defects of KBs. Further verification could be done by looking at the fracture surface of the samples to determine failure mode. Looking at the paste adhesive samples in fig 4.9 (c) and (d), the mold release results did not offer up much insight into the integrity of the joint with a 0.1 correlation factor, however, the grease samples in this case showed a strong negative relationship indicating that as the storage modulus increased, the failure load capability decreased. Further investigation on why this is the case may be needed since an inverse relation would be expected.

Next, we look at the loss modulus, which is the viscous response of the material. For the loss modulus, a higher peak may be associated to a poor interface. Looking at the paste samples in fig 4.10 (c) and (d), we see this association between modulus peak and structural integrity for both contaminants. There is a weak negative relationship between the failure load and the loss modulus in the paste samples, with mold release having a -0.7 correlation and grease a -0.6. As the modulus increases, the failure load appears to decrease within the samples. However, this relationship appears to be the opposite in the film samples. For the film sample in fig 4.10 (a) and (b), we can see for the mold release contaminated samples, the failure load

increase when the loss modulus increases and the grease samples appear to have no consistency at all with results scattered.

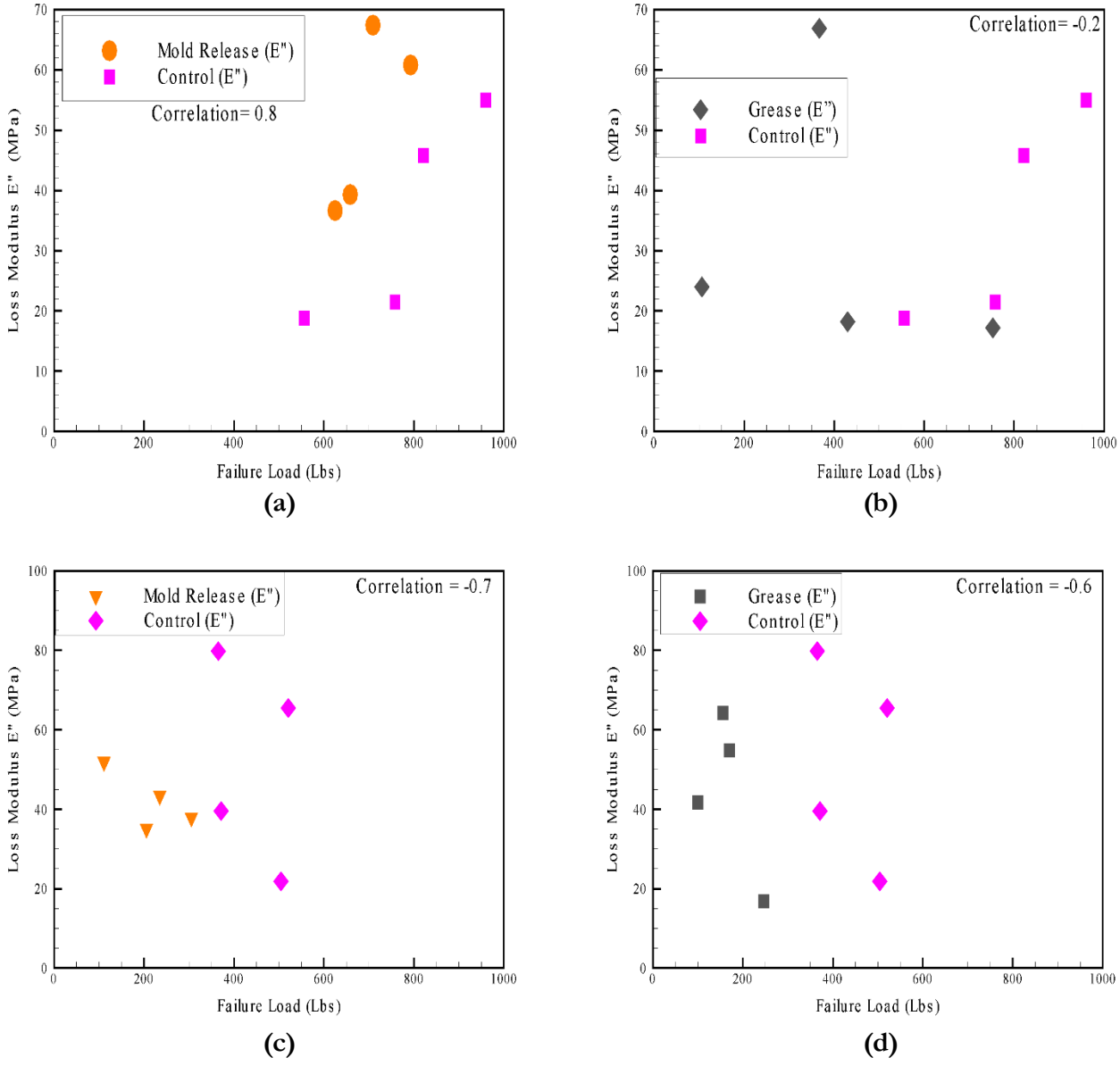

Figure 4.10: Loss Modulus vs Failure load for (a) Mold release film sample (b) Grease contamination film sample (c) Paste mold release sample, (d) Paste grease contamination

Several factors can damage and alter the stiffness of a structure. Therefore, by observing the correlation in the stiffness parameter measured in the DMA test versus the failure load between the reference parameters and that of the contaminated samples we hope to see a change that can be interpreted as indication that there is in fact a weak bond within the sample. Another factor that can affect the DMA results for the composite specimens' stiffness is the thickness of the specimen. In the case of this study, between the film and paste adhesive, the paste adhesive is known to have a thicker bond area as described in fabrication. We observed how that also played a role in the result illustrated in Figure 4.11. When looking at the results for the film adhesive samples in fig 4.11 (a) and (b), we do see a pattern between the strength and stiffness of each specimen. Within both the grease and the mold release samples, we can see that as the stiffness increase within the samples the strength increases so the amount of load they can withstand increases. However, for the mold release samples there wasn't a significant loss in stiffness compared to the control specimens, this doesn't necessarily signify that the sample does or does not contain a KB within its joint but it does open the door to further analysis.

When working with the paste adhesive, the opposite affect is observed within the results. Looking at fig 4.11 (c) and (d), we can see that as the stiffness decreases the bond strength reduces as well. However, the paste samples appear to have higher stiffness values than those of the film samples which could be attributed to the different material properties. Unlike the mold release specimens in the film plots, the specimens in the paste analysis did experience significant loss in stiffness when compared to the control specimens. The interaction between the contamination and the adhesive is very different for the two adhesives leading to very different results. Given the difference in material properties the joints will

behave differently when loaded, in chapter 5 we will take a closer look at the stress and strain distributions experienced within the joint for different adhesives.

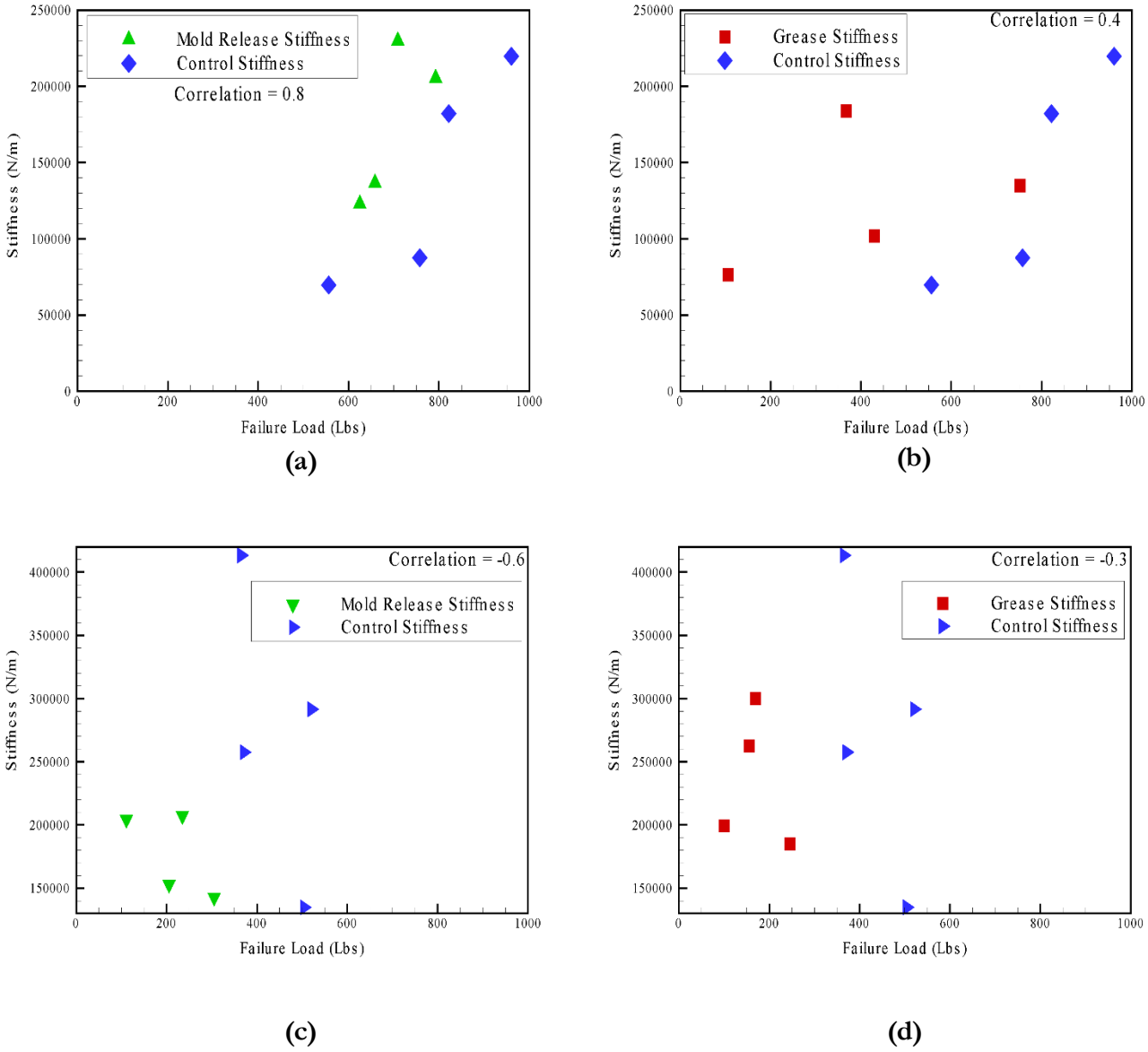

Figure 4.11: Stiffness vs Failure load for (a) Mold release (film) (b) Grease (film) (c) Paste mold release (d) Paste grease contamination

Next we analyzed the peak tan (δ) value and a reduced failure load. However, this is only evident in fig 4.12 (c) for the mold release paste samples. Compared to the control samples, all mold release samples did exhibit reduced load capabilities at higher tan (δ) peaks indicating that there possibly was weak bonding occurring within the joint area but the results were not conclusive within the remaining plots. For the grease paste samples in fig 4.12 (d), we do see some indication that as the tan (δ) peak increased the failure load capacity did decrease slightly but for the film samples in fig 4.12 (a) and (b) this was not the case. For the case of the film specimens, the increase in tan (δ) peak seemed to result in an increase in failure load capacity for both contaminants.

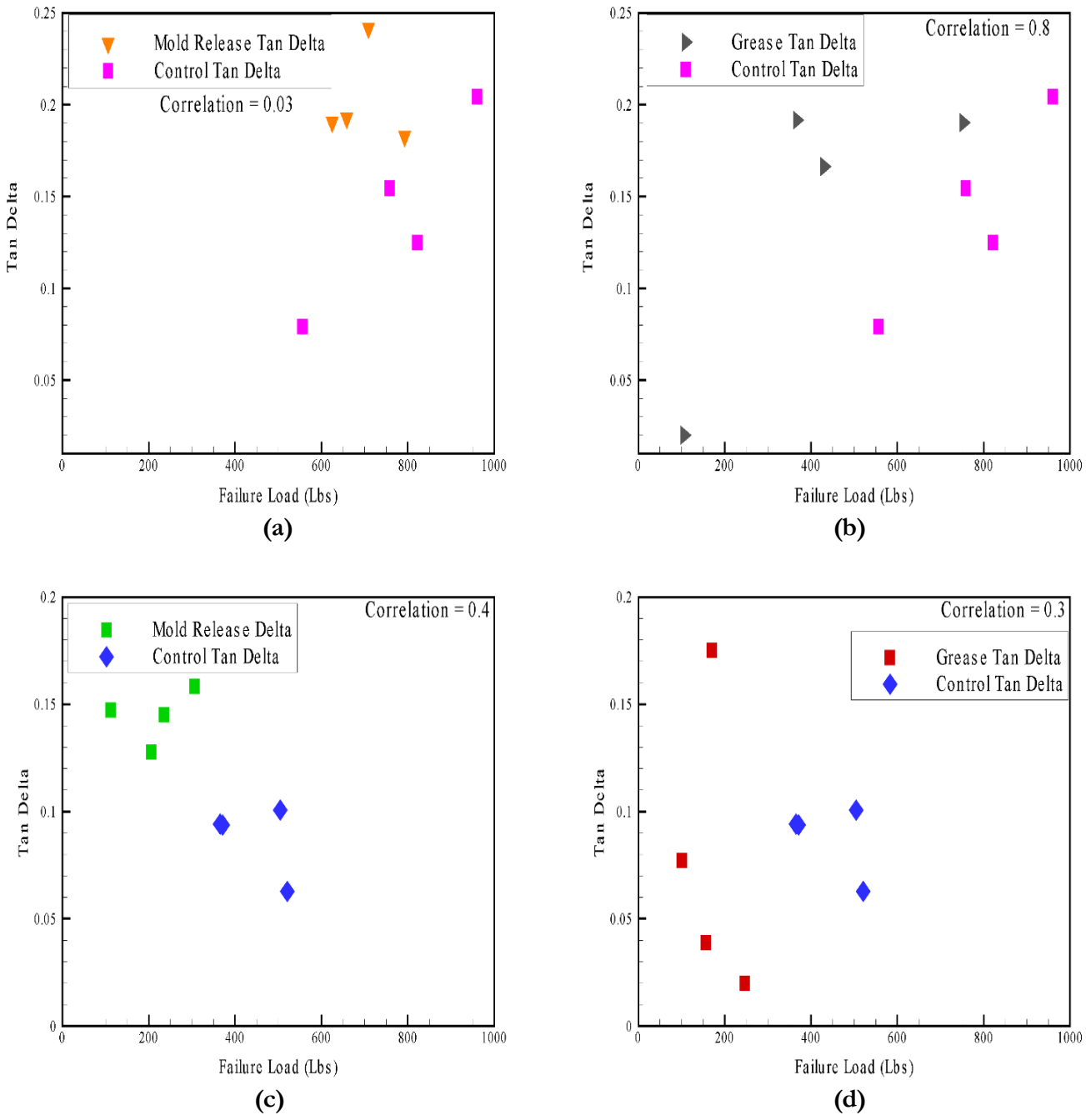

Figure 4.12: Tan (δ) vs Failure load for (a) Mold release film (b) Grease film (c) Paste mold release (d) Paste grease contamination

5. Finite element analysis

In this chapter, we will look at a simplified defect-free finite element models of the joint configurations evaluated in this thesis. A finite element (FE) analysis was conducted on two different adhesive joint models using ABAQUS (Dassault Systems, Providence, Rhode Island) software. The purpose of this work is to investigate the stress and strain distributions across the adhesive layer thickness in the SLJ test. A comparison of the stress distribution in the film adhesive and paste adhesively bonded joints is performed.

Table 5.1: Material properties used in finite element analysis of adhesive joints

Material	E GPa	Tension Strength (MPa)	v_{12}	G_{12} GPa
CFRP	57.98	-	0.037	4.00
Paste Adhesive	2.17	51.7	0.22	0.897
Film Adhesive	1.11	48.2	0.34	0.413

A 3D mesh comprised of plain strain elements was used for this analysis below. The FE solution was run using the geometric non-linear option to allow for large deformation effects to be properly handled. The materials used had linear elastic properties. Material nonlinearity was not included in the material model. The geometric nonlinear analysis was performed on the single-lap joint using 1374 plain-strain linear quadrilateral continuum elements (CPE4R) with 1638 nodes. The adherends' were modeled using isotropic material with properties shown in table 5.1, while the adhesives were modeled as an isotropic material, using properties obtained from manufactures catalog. The properties supplied by the manufacturer did not include plastic stress/strain curves, so true material non-linear analysis could not be performed. The dimensions of the FEA model were similar to the experimental specimen

dimensions illustrated in figure 3.2. Boundary conditions applied were similar to that found in experimental conditions; one end of the joint was completely constrained in all the degrees of freedom, while the other end was subjected to a 5mm controlled displacement along the x-direction. In studying the bondline thickness effects, simulations have been conducted on film and paste SLJ with adhesive thicknesses of 0.25 and 0.4 mm respectively. Two different mesh sizes were used to model the adhesive thickness. Mesh 1 consisted of 3-mesh elements for thickness 0.25 and 0.4 mm, and Mesh 2 consisted of 10 element analysis which was used to obtain more refined simulations for the same adhesive thicknesses illustrated in Figure 5.1 below.

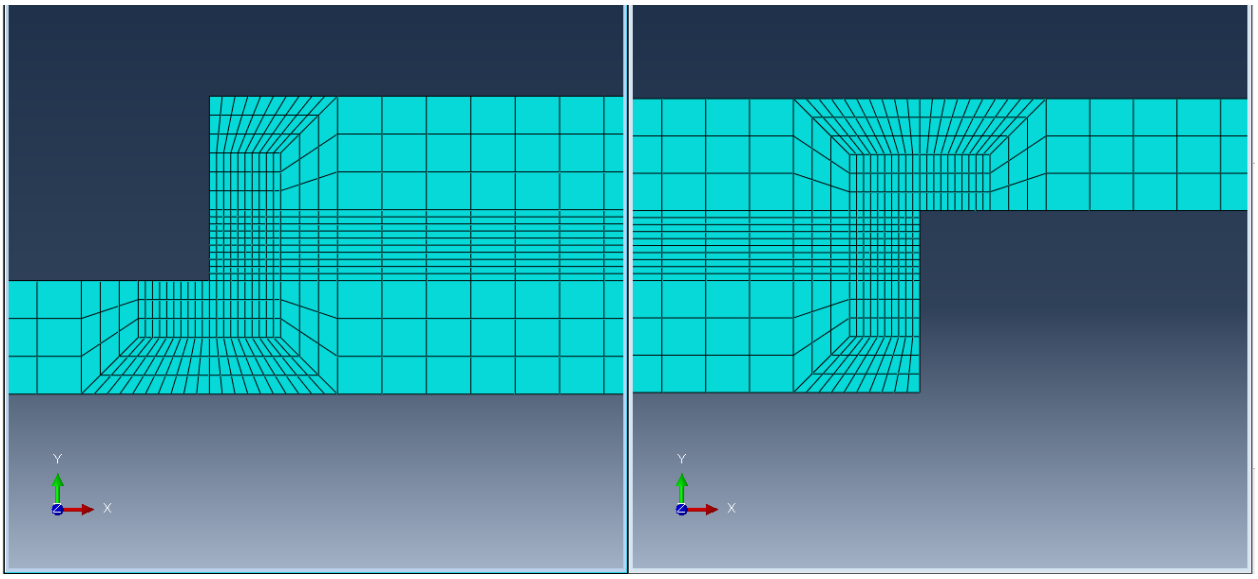

Figure 5.1: Schematic of mesh refinement, 10-element Mesh 2

Ideally there should be a uniform shear stress in the adhesive layer of an adhesive-bonded lap joint under tensile loading in order to give maximum joint efficiency [27]. However, this ideal is rarely achieved in practice because of stress concentrations due to three separate factors[27]:

- Differential straining in the adherends – the shear-lag effect
- Bending induced by non-axial loading
- End effects caused by the free surfaces at the edges of the adhesive layer

The shear stress and elastic strain response for a defect-free single-lap joint film adhesive configuration in tension loading with a 3-element mesh is illustrated in figures 5.2 through 5.5 below. Although many researchers have investigated the stress analysis of the single-lap joint for a long period, some controversial issues remain. For example, for the maximum shear stress, some results show it occurs at the free end of adhesive layer, while others show that it occurs at a short distance from the free ends [28]. In our model, we can see that the adherend and adhesive stress distribution in the overlap near the free surface are quite different from those stresses occurring in the interior. We can see in Fig 5.2, that the shear stress does not change significantly across the joint width. The stress concentration is higher at the edges of an adhesive joint due to geometrical discontinuity leading to strain localization in the region shown in Fig 5.4 and Fig 5.5. There is a strong strain concentration at the corners in the free edge of the overlap shown in these figures, we can see the beginning presence of peel that it occurs at a short distance from the free ends of the overlap region which will lead to failure in the joint. If cohesive bond failure is to occur, the present numerical simulation suggests the following failure mechanism that is the crack initiation will occur at these points, followed by the crack propagating along the film adhesive before both cracks join each other and propagate thru the adhesive thickness.

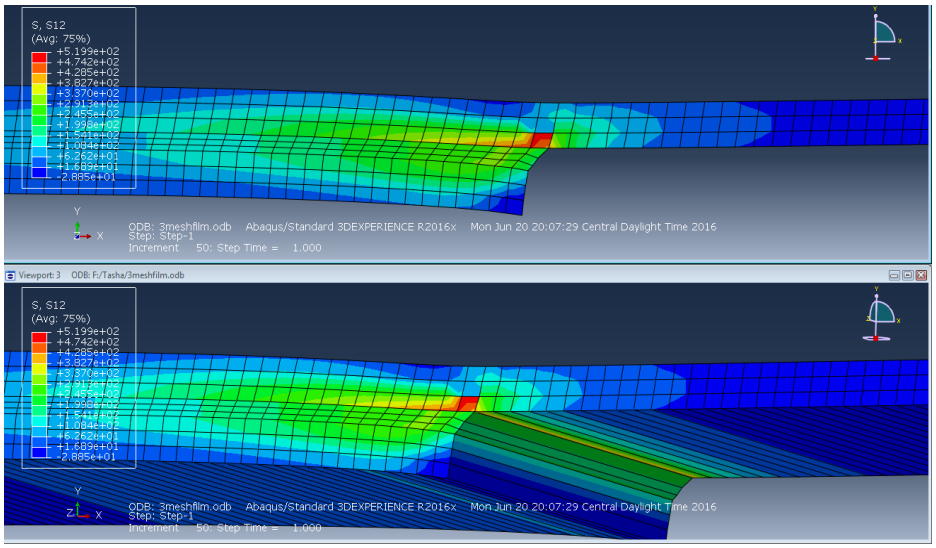

Figure 5.2: Shear stress distribution for film adhesive

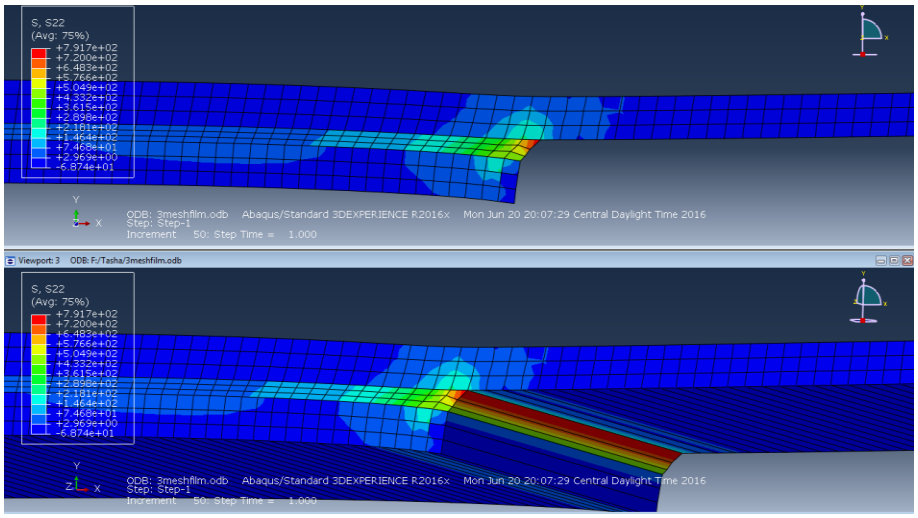

Figure 5.3: Peel Stress distribution for film adhesive

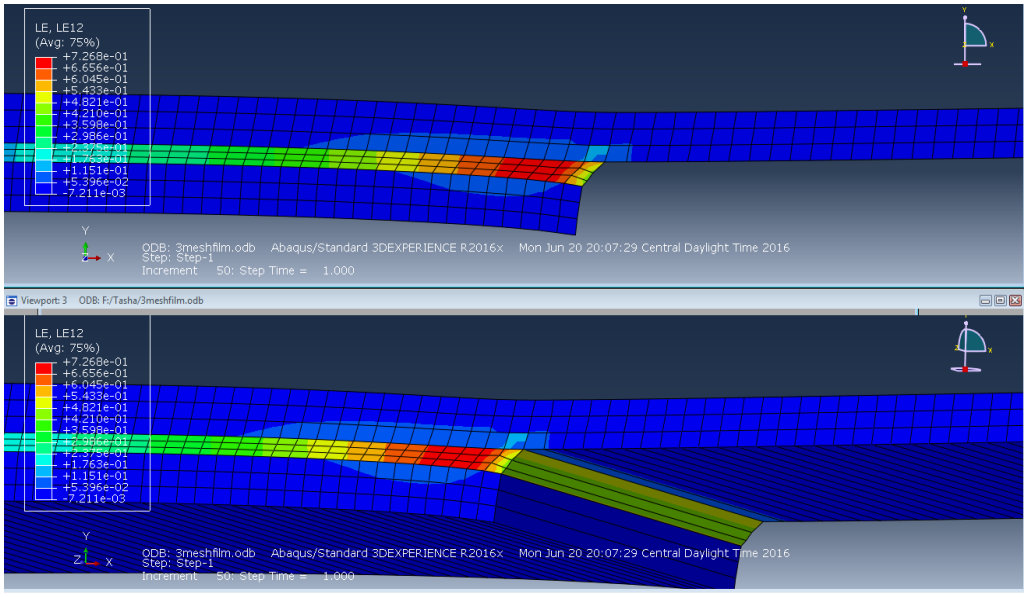

Figure 5.4: Shear strain distribution for film adhesive

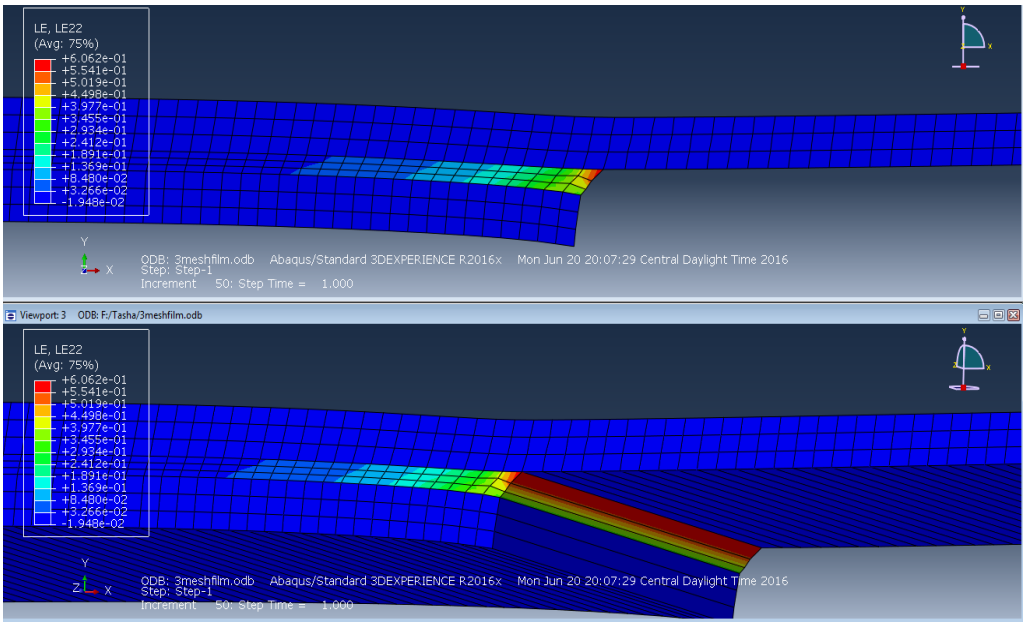

Figure 5.5: Peel strain distribution for film adhesive

The shear stress and elastic strain response for a defect-free single lap joint paste adhesive configuration with mesh 1 in tension loading is illustrated in figure 5.6 through 5.9 below. As previously stated, the paste adhesive is known to have a thicker bond area as described in section 3.2, and when looking at the stiffness results obtained from the DMA we can see that most of the paste samples had stiffness values much larger than the film samples.

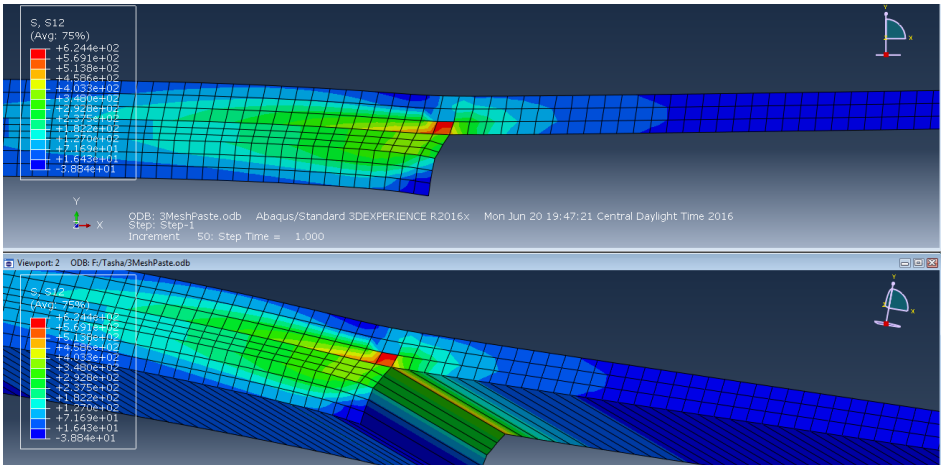

Figure 5.6: Shear stress distribution for paste adhesive

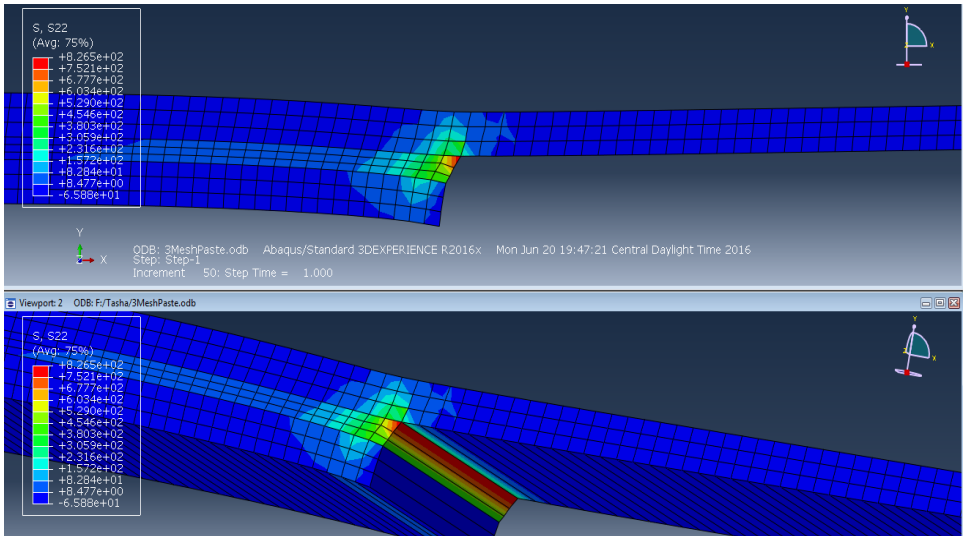

Figure 5.7: Peel stress distribution for paste

Comparing the max shear stress experienced by the film adhesive to that of the paste adhesive, we can see from Fig 5.6, the paste bond area is experiencing higher levels of stress. This increase could be due to the difference in material properties such as the Young's modulus. From the material properties we see that the paste adhesive had a larger Young's modulus, thus implying it is stiffer than the film adhesive which agrees with the results observed in section 4.5. However, the stain distribution is lower for the paste specimen which more than likely is attributed to the thicker adhesive layer within the SLJ. The regions near

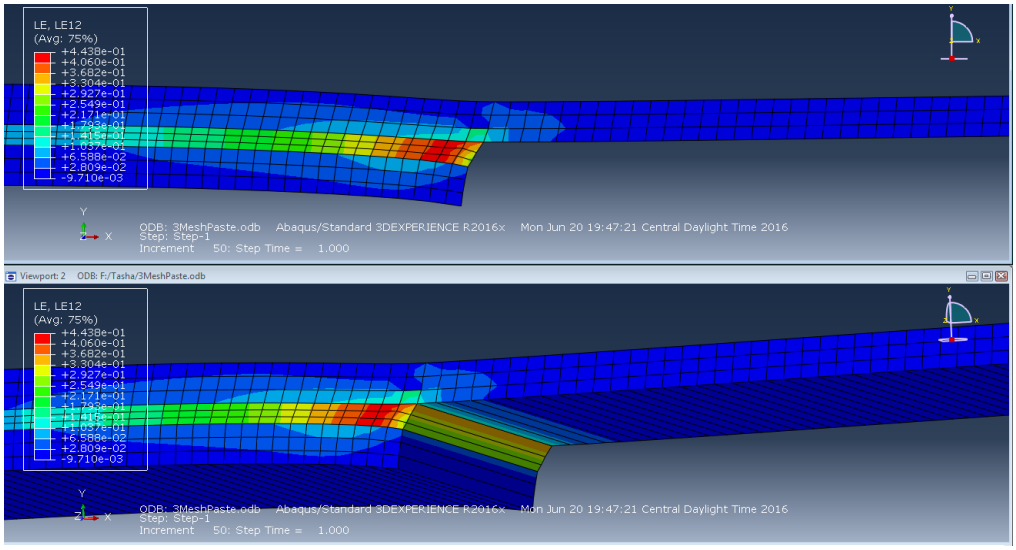

Figure 5.8: Shear Strain distribution for paste adhesive

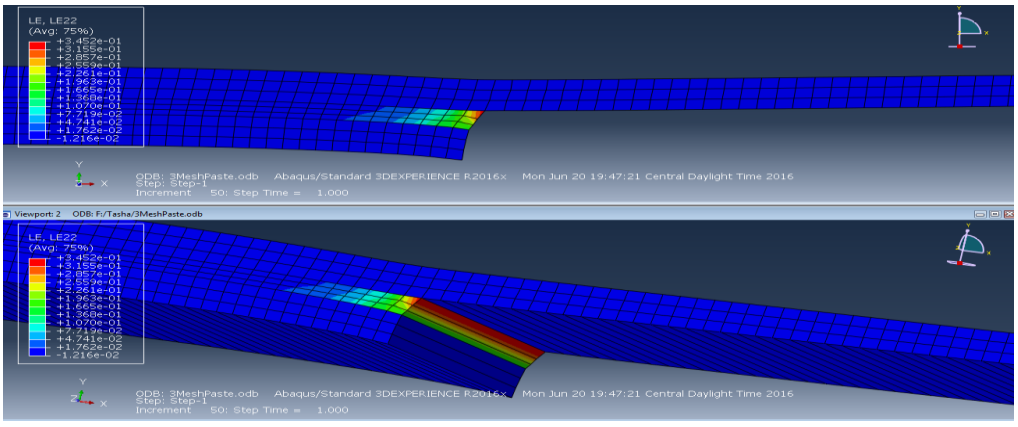

Figure 5.9: Peel Strain distribution for paste adhesive

the free edges appeared to be the most loaded and the region in the middle not as critical to

the bonded joint. Looking at the elastic strain distribution between the two adhesives, we can see that the thinner the adhesive thickness is the higher the strain value is for the SLJ. Next we analyzed the SLJ with 10-element mesh for both film and paste adhesive thicknesses respectively. The results are shown in figures 5.10 through figure 5.13 below.

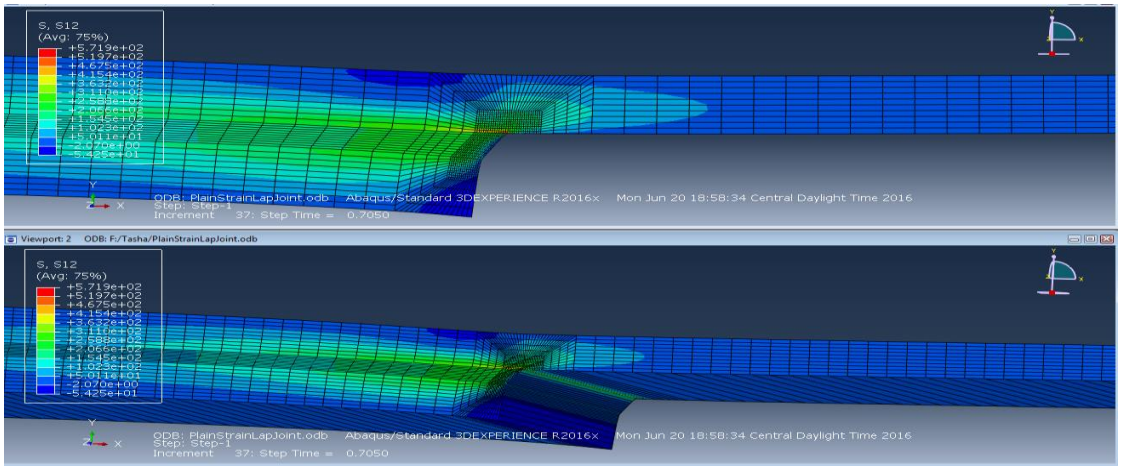

Figure 5.10: Shear Stress distribution along bond line for 10-element mesh film adhesive

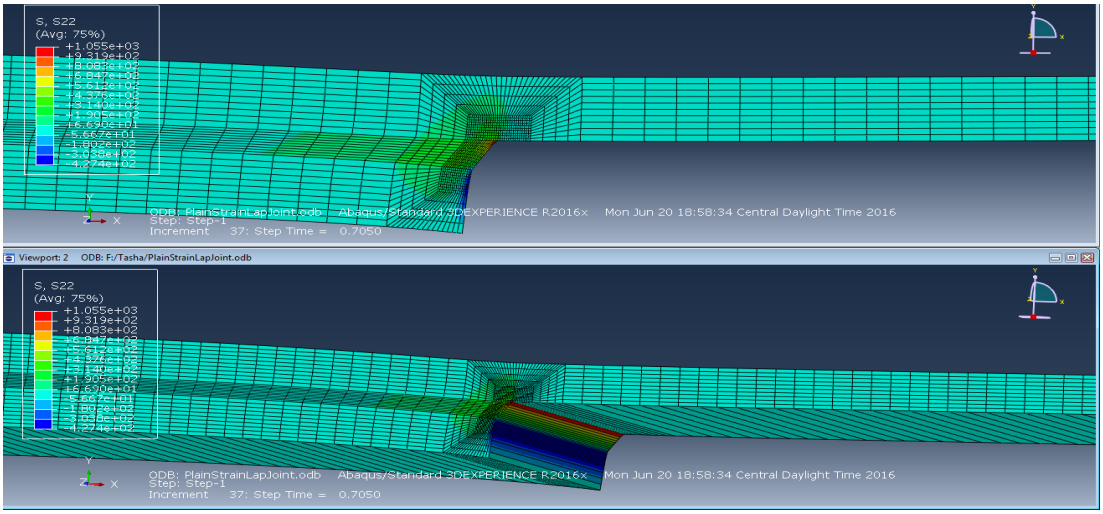

Figure 5.11: Peel Stress distribution along bond line for 10-element mesh film adhesive

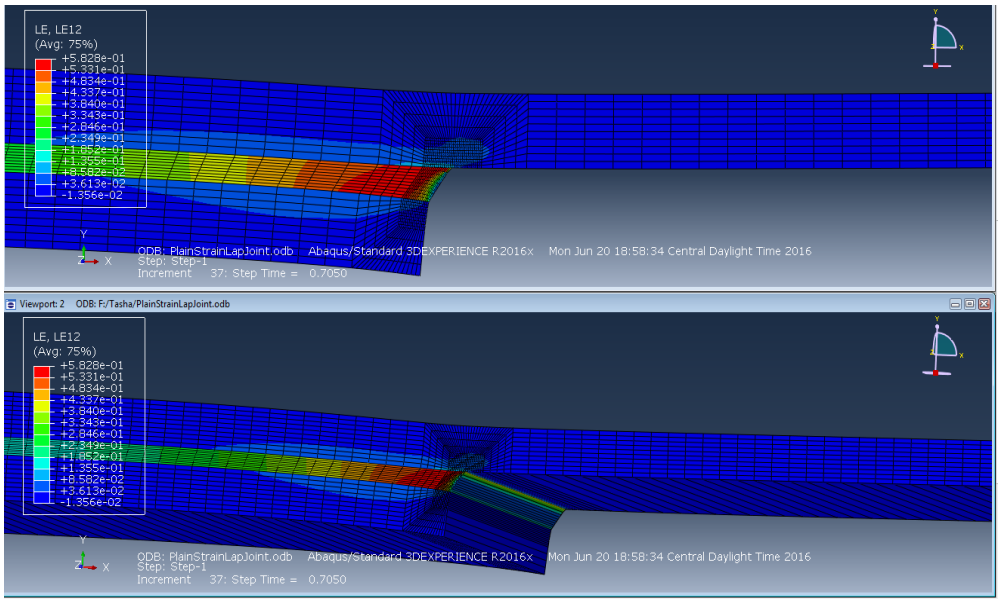

Figure 5.12: Shear strain distribution along bond line for 10-element mesh film adhesive

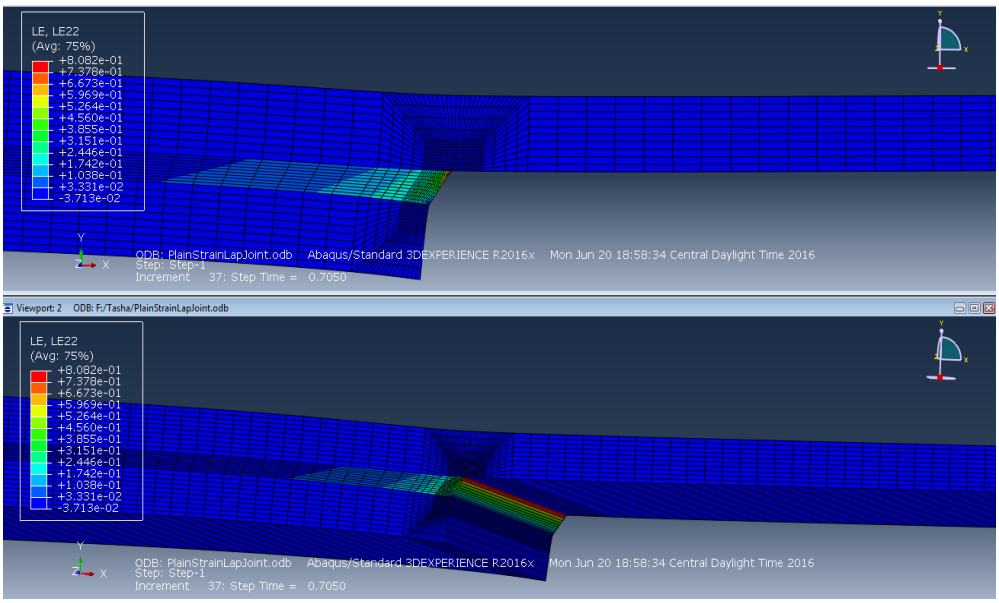

Figure 5.13: Peel strain distribution along bond line for 10-element mesh film adhesive

The shear stress and elastic strain response for a defect-free single lap joint paste adhesive configuration with mesh 2 in tension loading are illustrated in figure 5.14 through 5.17 below.

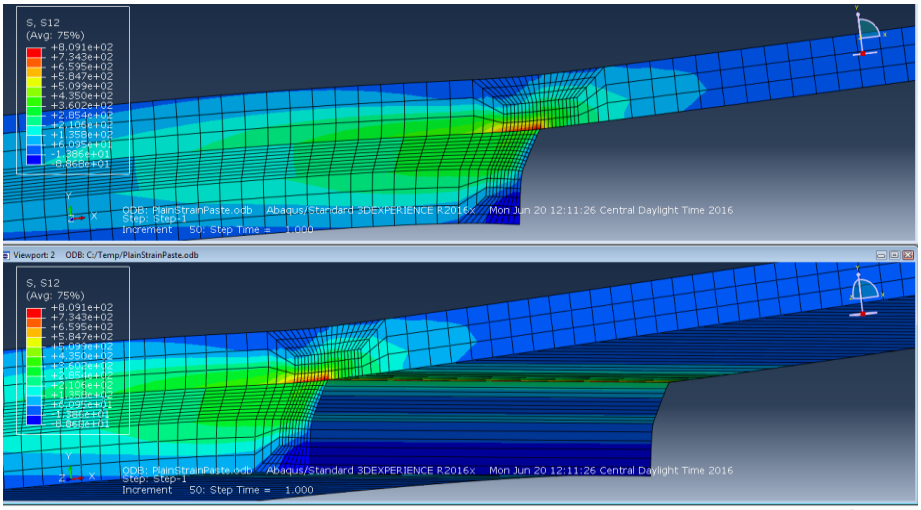

Figure 5.14: Shear Stress distribution along bond line for 10-element mesh paste adhesive

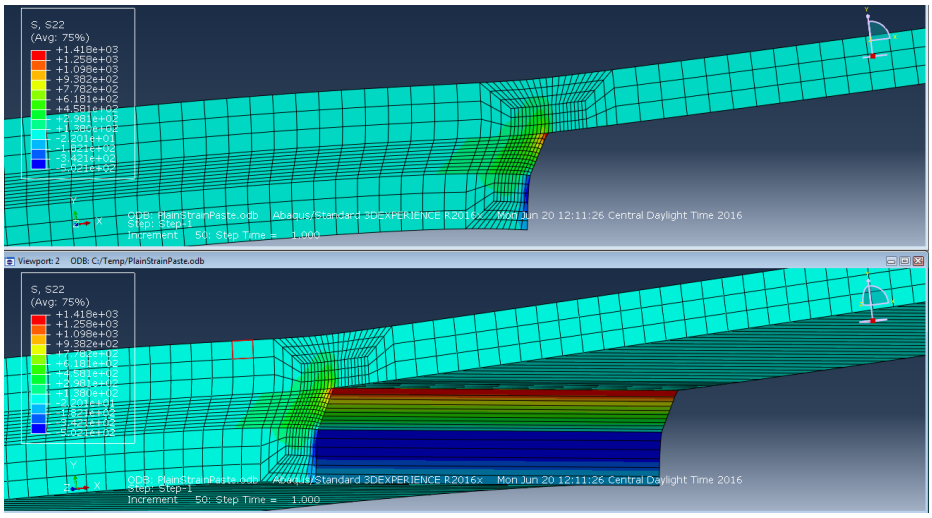

Figure 5.15: Peel stress distribution along bond line for 10-element mesh paste adhesive

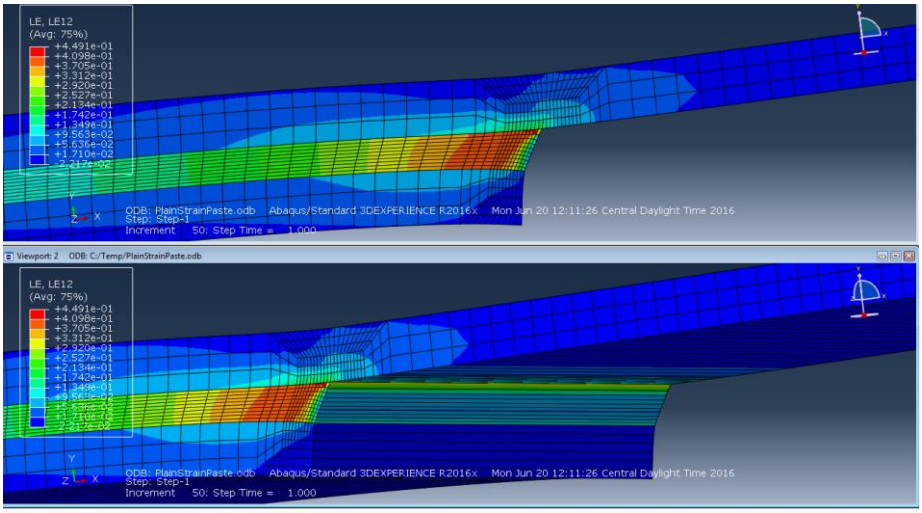

Figure 5.16: Shear strain distribution along bond line for 10-element mesh paste adhesive

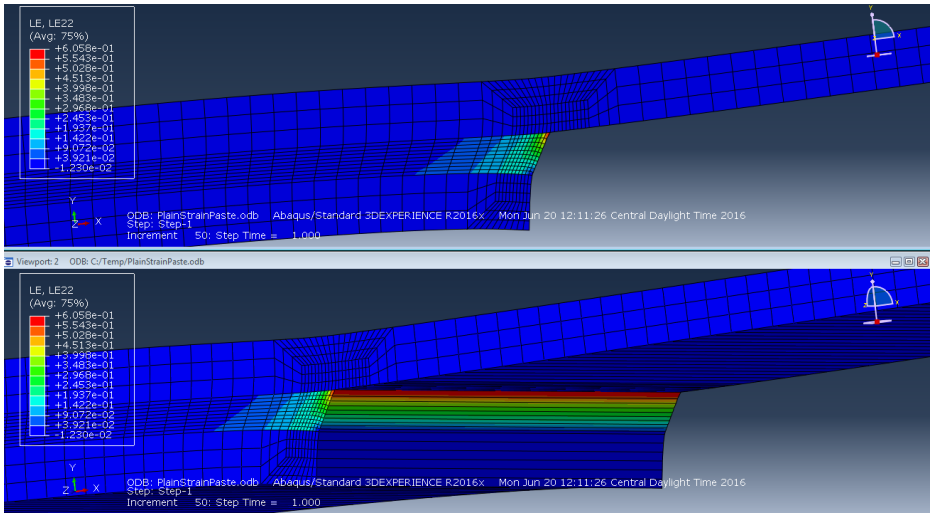

Figure 5.17: Peel strain distribution along bond line for 10-element mesh paste adhesive

With the refined 10-element mesh in the second model, we can see that there is an increase in shear and peel stress distribution within both paste and film adhesive models. As with the paste adhesive in mesh 1, we see the same occurrence happening within the paste adhesive with mesh 2, the strain within the SLJ is increasing. The FE results in Figure 5.18 and 5.19, show that the peel and shear stress at the overlap of the SLJ are significantly greater for the low stiffness film adhesive when compared to the paste adhesive SLJ. Increasing the

adhesive thickness resulted in a decrease shear strain distribution within the paste adhesive lap joint, as well as peel strain. The peel stress and shear stress distribution are within similar magnitude for both adhesives.

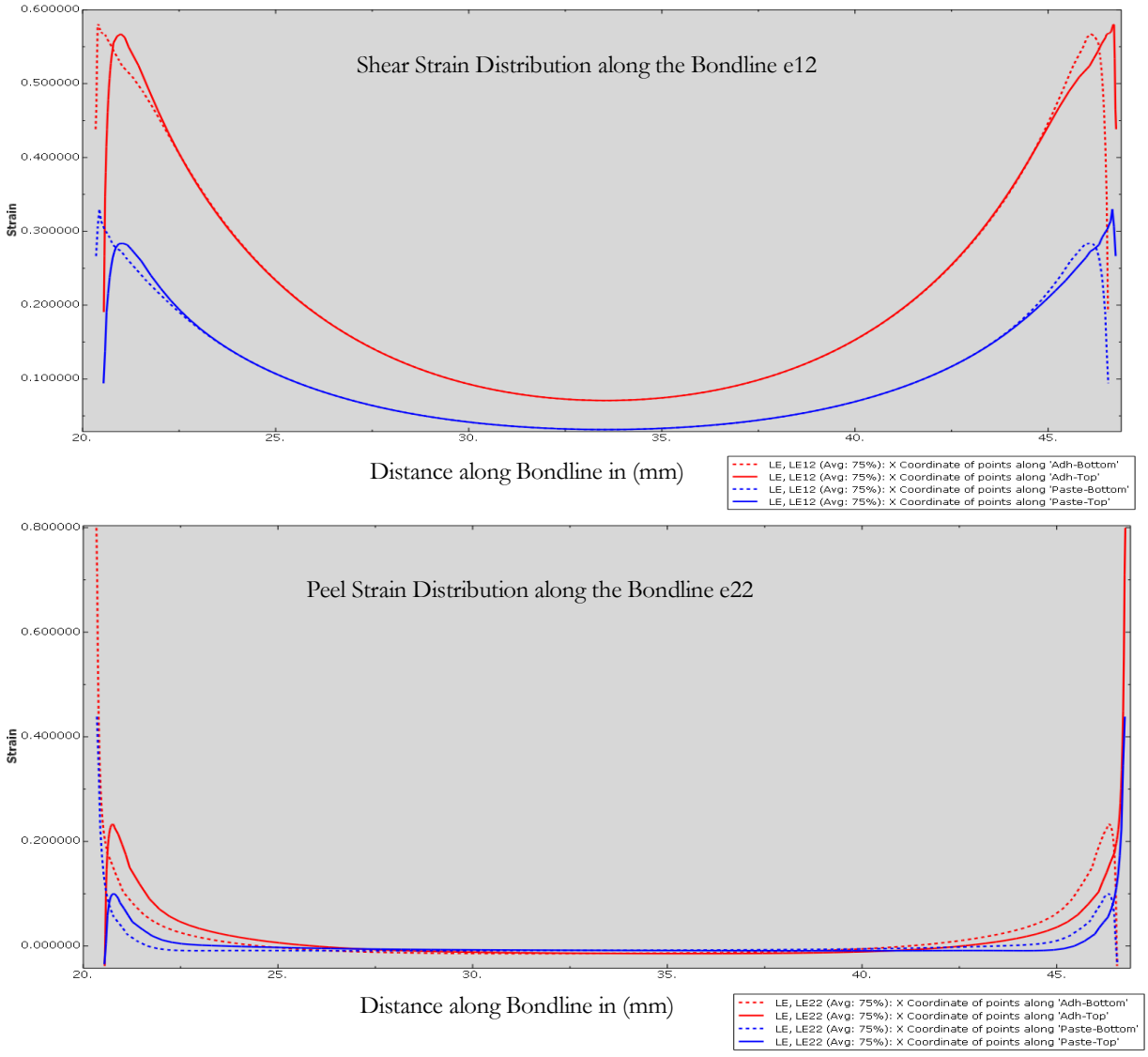

Figure 5.18: Peel and shear strain distributions for different adhesives

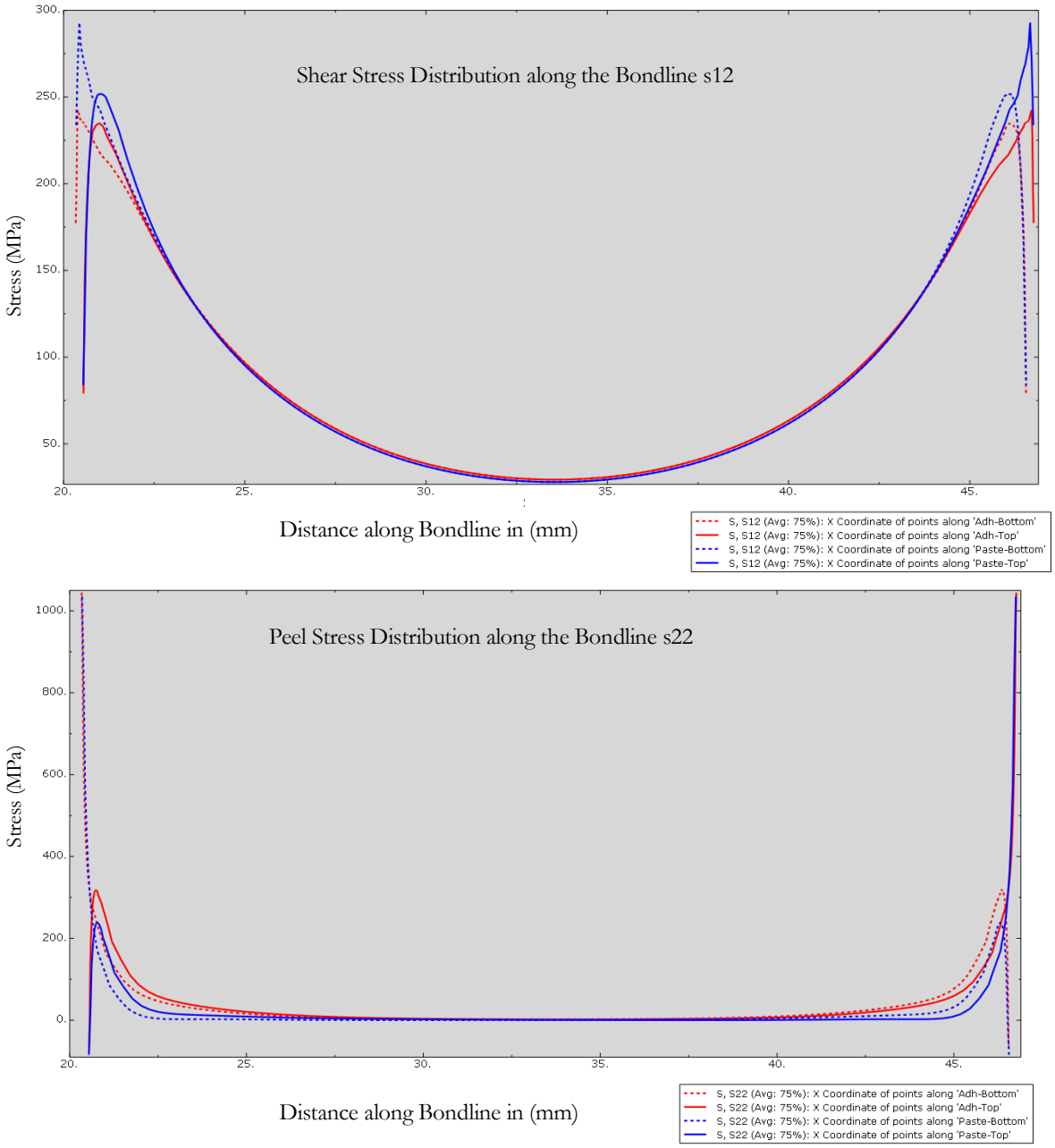

Figure 5.19: Peel and shear stress distributions for different adhesives

Using the same 3D mesh comprised of plain strain elements, the SLJ is loaded in bending instead of tension with an applied displacement of 15μm in order to understand the stress state in the DMA test. The shear stress and strain distribution for the paste and film adhesive are illustrated in figures 5.20-5.23 below.

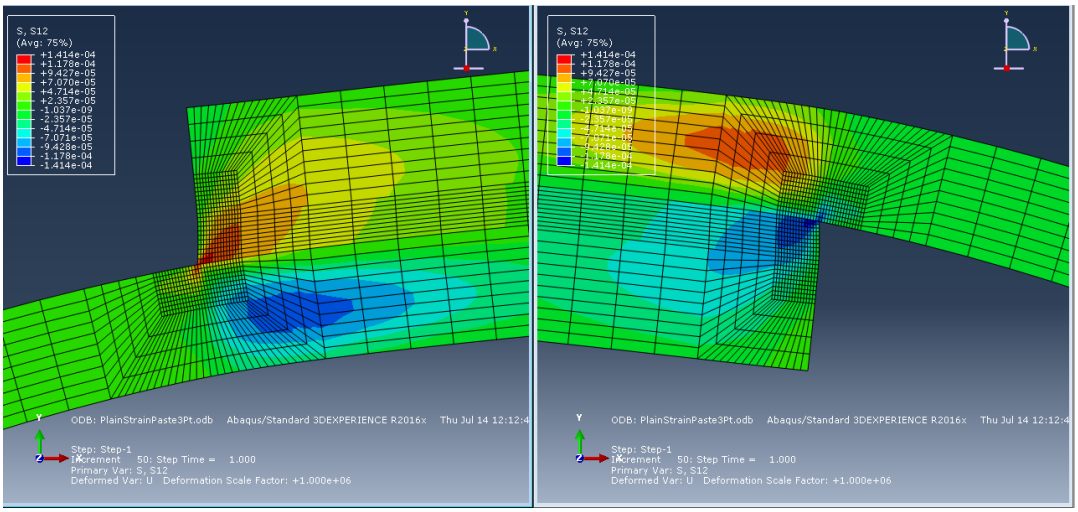

Figure 5.20: Shear stress distribution along bondline in bending loading for paste adhesive

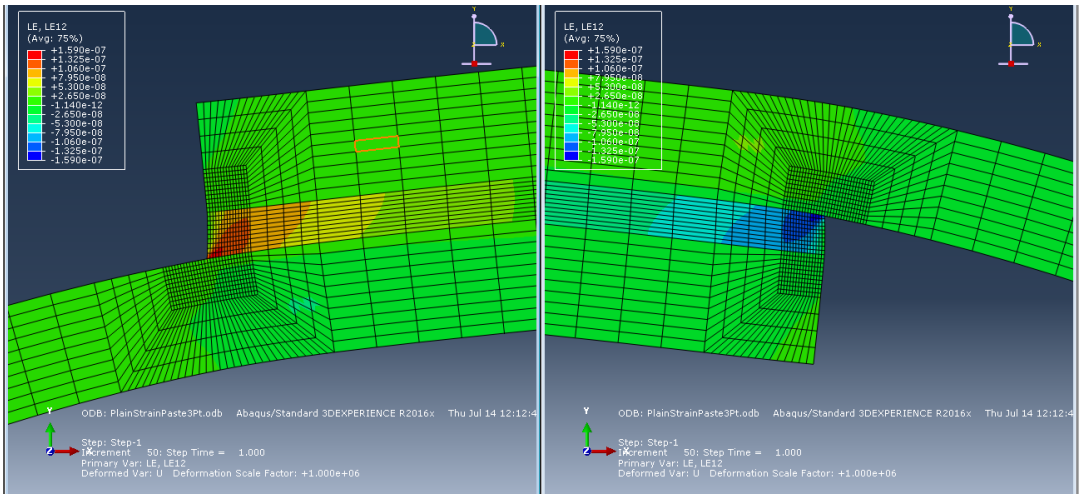

Figure 5.21: Shear strain distribution along bondline in bending loading for paste adhesive

When observing the stresses and strains within the specimen, we see the same trends that we observed in the tension testing. There is an increase in shear and peel stress distribution within that film lap joint and decrease in paste adhesive models and the concentration of stresses and strains are located at the free ends of the joints while the stresses

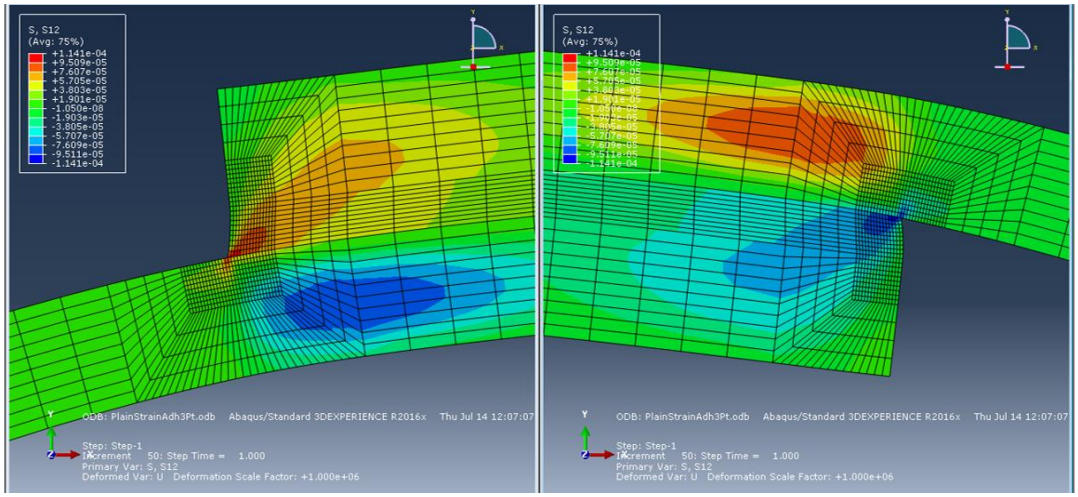

Figure 5.22: Shear stress distribution along bondline in bending loading for film adhesive

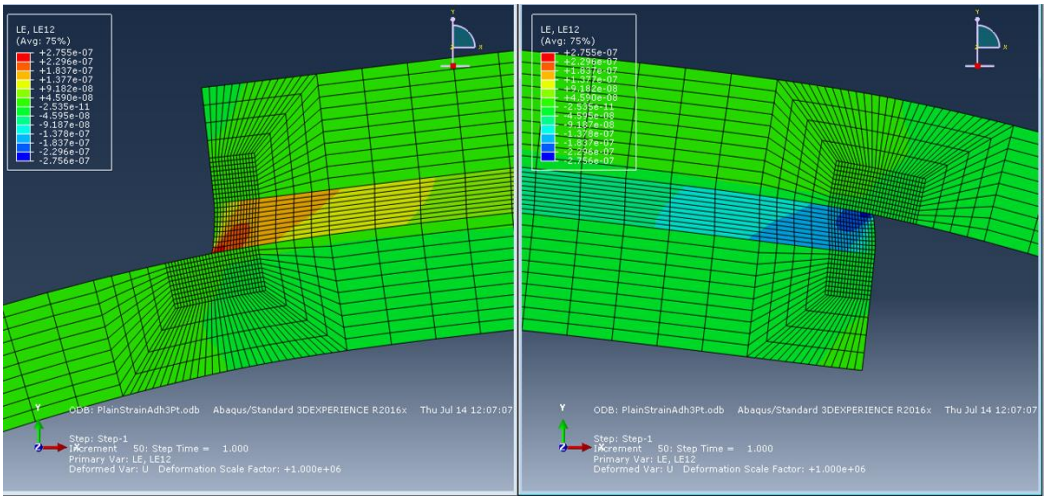

Figure 5.23: Shear strain distribution along bondline in bending loading for film adhesive

appear uniform within the bond area. Figures 5.24 and 5.25 illustrates the same conclusion for the stress and strain distributions graphically below.

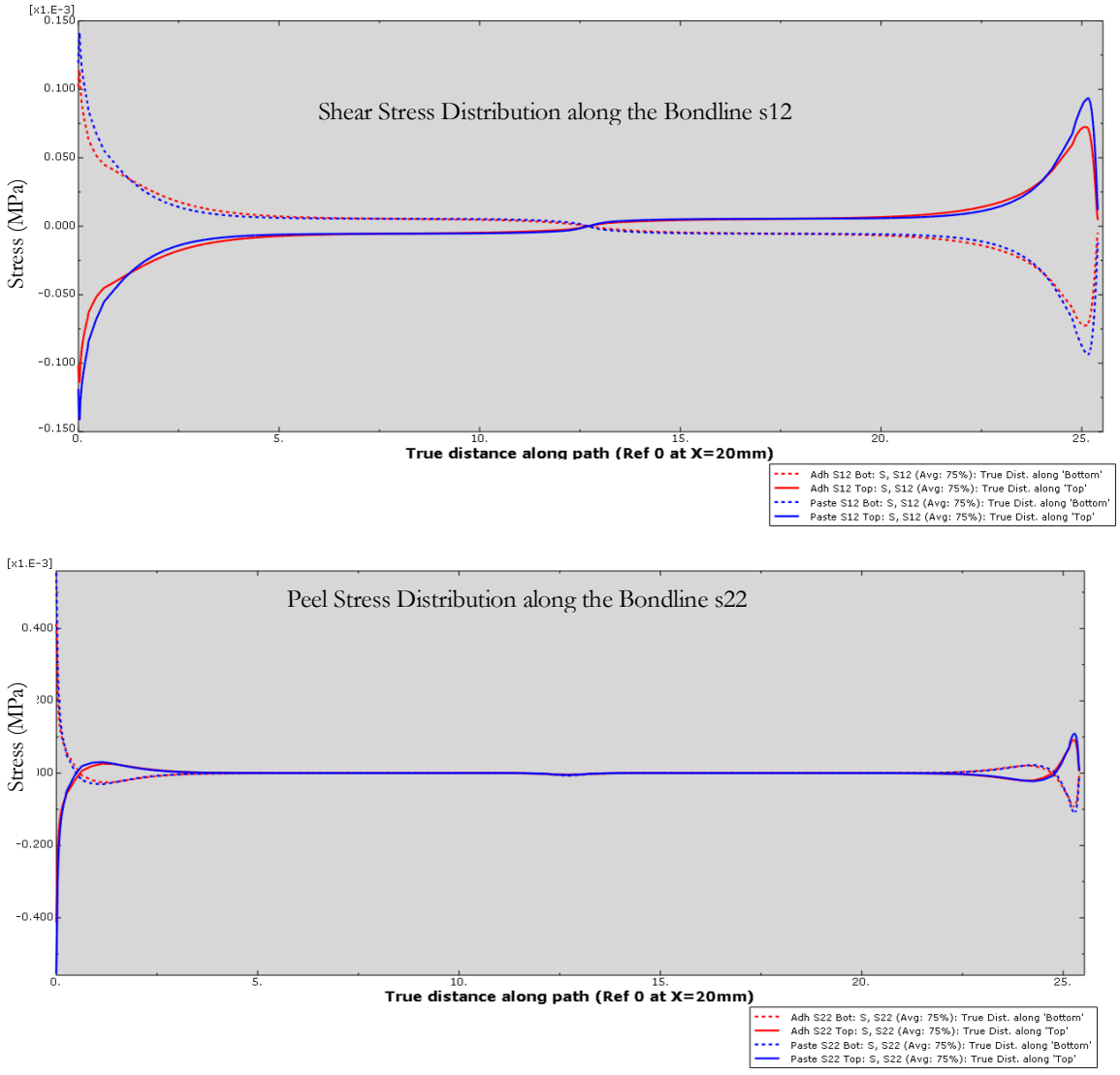

Figure 5.24: Peel and shear stress distributions for different adhesives

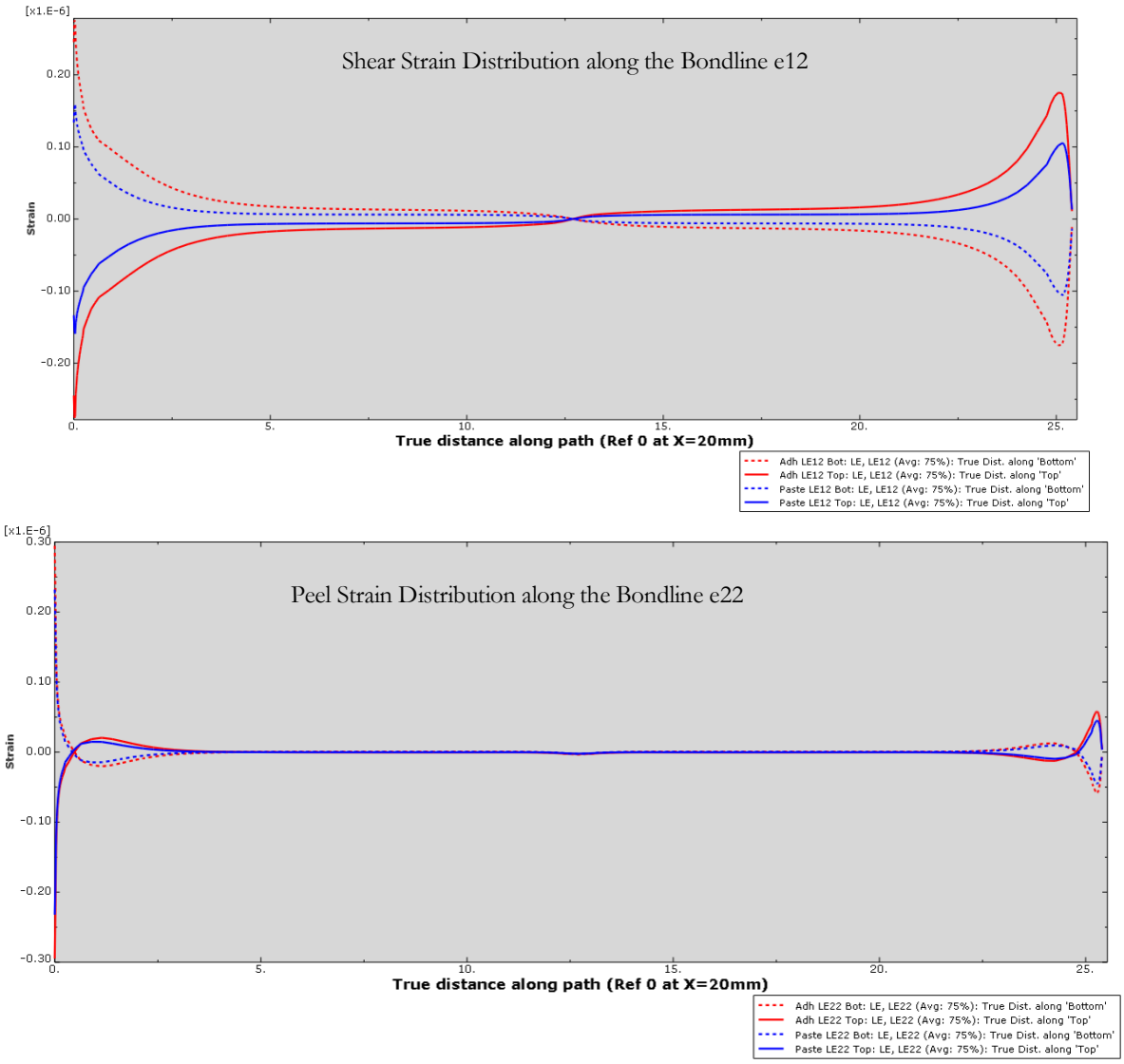

Figure 5.25: Peel and shear strain distributions for different adhesives

5.1. Summary

This finite element model of single-lap joint geometry was used to study the stresses and strains in the bonded area. The analysis has shown that the maximum peel stresses and corresponding strains occur away from the centerline. The stress state away from the edges of the overlap within the SLJ is relatively uniform. It is observed that the peak shear stress increase while the strain decrease with increase of the bond thickness and elastic modulus. FEM results showed that the stresses became increasingly higher within the single-lap joint for paste adhesive compared to the film adhesive. The paste samples are stiffer due to an increase in both tensile modulus and Young's modulus, but at the same time they were found to be more brittle when compared to the film samples so this change in stress and strain concentration could be attributed in part to the fact that they are sensitive to material properties. From section 4.5, we saw that film samples for the most part had higher storage modulus values which means it has a larger elastic energy which could potentially be attributed to the capability of the film samples indeed being more tolerant to the presence of defects than paste or they have a better chemical affinity between the adhesive and adherend than paste.

The maximum shear stresses and strains in both tension and DMA loading occur near the overlap joint corners ends, suggesting that cohesive crack initiation is most likely to occur at the corners for defect-free samples. From literature review [29], possible methods investigated in order to optimize the design of SLJs, was to taper the adherends (scarfing them), or to locally thicken the adhesive layer. These methods were tested and found to alleviate all three important stresses that govern the design such as peel, and shear stress.

6. Conclusions

In this study experimental investigations on evaluation of kissing bonds in composite adhesive lap joins was carried out on six different groups (3 for each adhesive type), one a defect-free and the other two defective samples with mold release and grease contaminations. Defect detection is currently better developed than the understanding of the significance of what has been detected. The integrity of adhesive joints must therefore be ensured by tests carried out before bonding to ensure that surface preparation is satisfactory and by very careful process quality control [19].

The focus of this work was the contamination effect on the adhesively bonded joints. It is found that the contamination has effects on both the interfacial bonding strength and the adhesive mechanical properties. The specimens were first tested with DMA in the hope of detecting localized weakness within the bonds of two different adhesives-type lap joints. Then it was demonstrated that the load carrying ability of the single lap shear joints decreased due to the introduction of surface contaminants in the bonding substrate by conducting tension testing. During tension testing, it was seen that for the film samples, the grease contaminant reduced the shear strength by roughly 46% while the mold release only reduced the shear strength by approximately 10%. For the paste samples, the grease contaminant reduced the shear strength by approximately 62% and the mold release by 51%. A mixture of failure modes was observed within the samples; adhesion or mix-mode failures are due to degradation of the interface and indicate a reduction in bond strength. From the results obtained from testing for both contamination scenarios, it was seen that they create defects in the form of weak bonds that cannot be detected by means of conventional ultrasonic testing. Nevertheless, ultrasonic inspection tests were conducted prior to mechanical testing in order

to assess the quality of the bondline. Among the parameters obtained from DMA testing, storage modulus, stiffness and tan (δ) provided reasonable correlation for some parameters when compared to failure stress from the SLJ tests. In the case of the storage modulus, we saw strong correlations among the mold release samples in film adhesive and the mold release samples in paste both with a 0.7 and 0.8 correlation coefficients respectively. The grease samples in the film SLJs are scattered and had a correlation strength of 0.1. Among the stiffness parameter, the film mold release samples had a strong correlation of 0.8, and demonstrated the trend of increase strength with increase in stiffness, while the paste mold release samples had a -0.6 correlation value and demonstrated an opposite trend with the failure load decreasing with increasing stiffness. Lastly, the tan (δ) parameter had strong correlation among the mold release contaminant in the paste SLJs, with a correlation value of 0.6.

It was seen from the FEA models that the maximum shear stress and elastic strain occur near the overlap joint corners ends, suggesting that cohesive crack initiation is most likely to occur at the corners for defect-free samples. The stiffness results obtained from the DMA showed that the paste samples all had stiffness values much larger than the film samples, this was evident in the FE models as well as we can see the level of strain increase in the paste model compared to that of the film. However, the stresses were higher in the paste adhesive specimens and may have contributed to the higher reductions when defects are present.

6.1. Suggestions for future research

In order to fully verify the findings of this thesis, a deeper analysis into the correlation between the parameters obtained from DMA testing and the results obtained from the SLJ testing is needed. The results encourage further testing on a larger data set of each type of contaminant in order to address the issues and understand the qualitative correlation between measured parameters and the presence of KBs. Running the experiment with larger varying displacements could also be beneficial in order to see how stresses and strains change within the joint, as well as to see if better results are obtained from the parameters explored since it may distort the weak bond and make its presence more apparent

REFERENCES

1. Broughton, W.R., *Assessment and Criticality of Defects and Damage in Adhesively Bonded Composite Structures*. 2016, National Physical Laboratory.

2. Caminero, M.A., *Damage monitoring and analysis of composite laminates with an open hole and adhesively bonded repairs using digital image correlation.* Composites: Part B, 2013: p. 76-91.

3. Katnam, K.B., L.F.M. da Silva, and T.M. Young, *Bonded repair of composite aircraft structures: A review of scientific challenges and opportunities.* Progress in Aerospace Sciences, 2013: p. 26-42.

4. Ehrhart, B., B. Valeske, and C.-E. Muller, *Methods for the quality Assessment of Adhesive Bonded CFRP Structures- A resume*. 2010, NDT in Aerospace: Saarbruecken, Germany.

5. Tighe, R.C., J.M. Dulieu-Barton, and S. Quinn, *Identification of kissing defects in adhesive bonding using infrared thermography*International Journal of Adhesion & Adhesives, 2015: p. 168-178.

6. Poveromo, S. and J. earthman, *Analysis of "Kiss" Bonds between composite laminates.* The Minerals, Metals & Materials Society 2014.

7. Brotherhood, C.J., B.W. Drinkwater, and F.J. Guild, *The effect of compressive loading on the ultrasonic detectability of kissing bonds in adhesive joints.* Nondestructive Evaluation, 2002. **21**(3): p. 95-103.

8. Roach, D. and K. Rackow, *Innovative use of adhesive interface characteristics to non destructively quantify the strength of bonded joints.*, in *European Conference on Nondestructive Testing*. 2010: Moscow Russia.

9. Davis, M. and A. McGregor, *Assessing Adhesive Bond Failures: Mixed-Mode bond failure explained* Adhesion Associates, 2010: p. 1-12

10. Markatos, D.N., *Experimental investigation of the effect of defects, non-detectable by means of conventional non destructive techniques, on the mode I fracture toughness of adhesively bonded composite joints*, in *DEPARTMENT OF MECHANICAL ENGINEERING AND AERONAUTICS*. Markatos,Dionysios N. , UNIVERSITY OF PATRAS.

11. Marty, P., D. N, and A. J, *NDT of kissing bonds in aeronautical structutres*, in *Proceedings of 16th world conference*. 2004: Montreal Canada.

12. Price, D. and P. Haines, *principles of Thermal Analysis and Calorimetry*. 2002: Royal Society of Chemistry. 236.

13. Foreman, J., *Dynamic Mechanical Analysis of Polymers*. 1997, TA Instruments.

14. *Dynamic Mechanicsl Analysis (DMA): A Beginner's Guide*. 2013, PerkinElmer: Waltham, MA.

15. Yang, P. *Dynamic Mechanical Characterization of Manufacturing Defects in Continuous Carbon Fiber/Epoxy Composites.*, in *SAMPLE*. 2014, Society for the Advancement of Materials and Process Engineering: Seattle WA.

16. Yang, S., *Nondestructive detection of weak joints in adhesively bonded composite structures.*Composite Structures, 2001. **51**: p. 63-71.

17. Ornaghi, H., A. Bolner, and R. Fiorio, *Mechanical and Dynamic Mechanical Analysis of Hybrid Composites Molded by Resin Transfer Molding* Journal of Applied Polymer Science, 2010. **118**: p. 887-896.

18. Olympus., *Applying Ultrasound*.

19. R.D. Adams, *Defect types and non-destructive testing techniques for composites and bonded joints.* Construction and Building Materials, 1989. **3**(4): p. 170-183.

20. Nagy, P., *Ultrasonic detection of kissing bonds at adhesive interfaces* Journal of Adhesion Science and Technology., 1991. **5**(8): p. 619-630.

21. Pantelakis, S. and K.I. Tserpes, *Adhesive bonding of composite aircraft structures: Challenges and recent developments.* Science China Physics, Mechanics & Astronomy, 2013. **57**(1): p. 2-11.

22. Markatos, D.N., et al., *The effects of manufacturing-induced and in-service related bonding quality reduction on the mode-I fracture toughness of composite bonded joints for aeronautical use.* Composite: Part B2013. **45**: p. 556-564

23. Seyedmohammad. S. and R. El-Hajjar, *Overlay patch repair of scratch damage in carbon fiber/epoxy laminated composites.* Composites, 2013. **49**: p. 148-156.

24. HUNTSMAN, *Epibond 100 A/B aerospace structural adhesive, technical data sheet. 2013*.

25. Light, G.M. and H. Kwun, *Nondestructive Evaluation of Adhesive Bond Quality*. 1989: Nondestructive testing information analysis center.

26. Simon, S. *What is Correlation*. Available from: http://www.pmean.com/definitions/correlation.htm.

27. Peppiatt, N.A., *Stress analysis of adhesive-bonded lap joints.* Journal of strain analysis, 1974. **9**(3): p. 185-196.

28. Her, S.-C., *Stress analysis of adhesively-bonded lap joints.* Composite Structures, 2000. **47**: p. 673-678.

29. He, X., *A review of finite element analysis of adhesively bonded joints.* International Journal of Adhesion and Adhesives, 2011. **31**.